Quantum Path Computing: A Low Complexity Quantum Computing Architecture with Feynman Path Integrals and Quantum Superposition*

Burhan Gulbahar

Department of Electrical and Electronics Engineering, Ozyegin University, Istanbul 34794, TURKEY

(Dated: September 5, 2017)

Double slit interference experiment is at the heart of quantum mechanics by clearly presenting quantum nature of particles such as electrons, photons, neutrons and molecules as emphasized by Richard Feynman. In this article, Feynman path integral formalism and quantum superposition of propagating particles are combined in a multi-plane and multi-slit based interference set-up to present a novel quantum computing (QC) architecture denoted by quantum path computing (QPC) without utilizing qubits and gate operations but exploiting superposition interference on the intensity distribution on the sensor planes. Hidden subgroup problem (HSP) is solved with a period finding solution in complete analogy with the existing period finding algorithms utilizing qubits and quantum gate structures. The system is used as a promising step for the solution of NP-hard simultaneous Diophantine approximation problem in algebraic number theory and non-uniform reciprocal integer lattices. Simulation results taking into account effects of exotic and non-classical paths show feasibility of QPC for providing quantum computational speed-up. QPC is an alternative architecture to existing QC methods having the challenges of noise, decoherence, high complexity of hardware and low number of qubits. It provides a low complexity design, low cost and room temperature operation as a promising step to realize polynomial solutions to some sets of computational problems requiring exponentially complex resources of time and memory.

Keywords: Quantum computing, Feynman path integrals, interference, NP-hard, simultaneous Diophantine approximation, non-uniform integer lattice, polynomial complexity.

I. INTRODUCTION

The Young's double slit experiment is one of the fundamental experiments where the foundational laws and the essence of quantum mechanics are contained as emphasized by Richard Feynman with detailed models for the electron based system set-up [1]. The importance given to the experiment by Feynman motivates to create a simple system design exploiting fundamental laws of quantum mechanics such as quantum superposition and Born rule to realize low complexity quantum computing (QC) architectures. QC architectures are recently promising quantum supremacy by utilizing qubits based on a rich set of materials including superconducting structures, quantum dots or trapped ions [2], annealing based adiabatic architectures [3] and topological quantum computing intrinsically error-protected by utilizing non-Abelian anyons [4]. The most fundamental problems in traditional systems are the noise with imperfections in quantum operations and the decoherence due to entanglement of qubits with the outside environments [5]. Furthermore, operation temperature, complexity of the hardware and small number of qubit realizations are other fundamental challenges in existing systems. Exploiting quantum superposition without utilizing qubit operations and gates achieves better protection from the noise and decoherence. The proposed solution denoted by quantum path computing (QPC) is an alternative QC architecture to existing academical and commercial prototypes. QPC

satisfies fundamental features of naturally inspired architectures combining simplicity, adaptability to different interference environments of particles including photons, low complexity and low cost architecture of the device operating at room temperature [6]. It exploits the superposition of significantly large number of operations with a simple design instead of complicated set-ups to realize high number of qubits and reliable quantum circuit gates.

The double slit experiments are recently getting more attention to analyze exotic paths of particles, Gouy phase effect in measurement of the Sorkin parameter and the fundamentals of Born rule [7–10]. The simplicity of slit based interference experiments and their experimental verification in recent studies further support experimental feasibility of QPC design.

Besides that, there are studies utilizing interference for factoring problems. Implementation of Gauss sum with optical interferences and Talbot effect produced by laser pulses are discussed in [11]. N-slit classical interferometer by using monochromatic light interference on a single plane and the similar design with Mach-Zehnder interferometer are presented in [12] and [13], respectively. Multi-path interference patterns with Michelson interferometers, generalized truncated Fourier sums with Mach-Zehnder interferometers and similar set-ups are shown in [14, 15]. However, these systems do not include multiple planes to form exponentially increasing number of paths while requiring exponentially large resources. They are not modeling the accurate interference patterns by using Feynman's path integrals and exotic paths, not targeting the simultaneous Diophantine approximation (SDA) problems and not providing a direct one-to-one analogy with the period finding traditional QC algorithms.
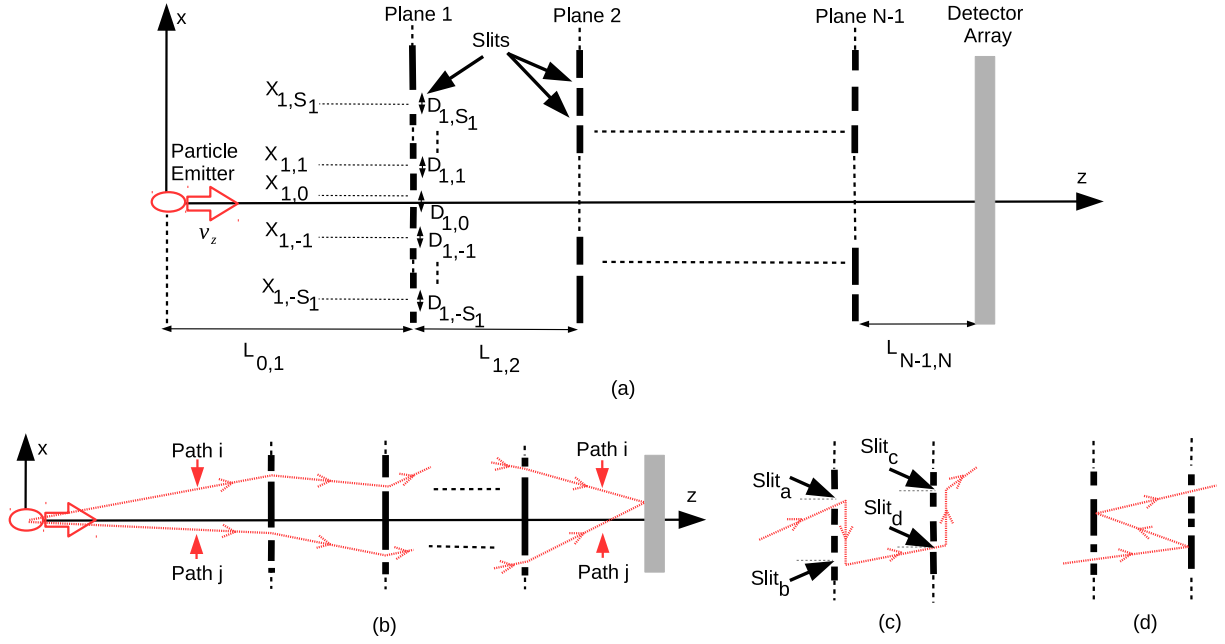
* burhan.gulbahar@ozyegin.edu.tr

FIG. 1. (a) Quantum superposition interference and quantum path computing (QPC) architecture with multiple, consecutive and parallel planes of slits, (b) ith and jth paths interfering on the detector array, and (c) exotic path among the slits with indices a, b, c and d, and (d) reflecting paths between the consecutive planes of the slits.

In this article, a simple set-up based on quantum superposition interference of fundamental particles due to multiple planes with multiple slits is utilized to create a QC solution of the period finding type for hidden subgroup problems (HSPs). The analogy with traditional period finding quantum algorithms utilizing qubits and quantum gates is explicitly provided promising QPC as a fundamental tool to be utilized in future computing architectures. QPC provides a theoretical model for accurate solutions of SDA problems with scalable count of real numbers as NP-hard problems in algebraic number theory with many applications in computer science, optimization theory and communications technologies. It is a low complexity, simple, low cost and room temperature QC architecture utilizing quantum superposition of exponentially increasing number of paths with respect to the number of planes and slits. Numerical simulations are performed by also accurately considering the effects of exotic paths discussed in [7–10]. QPC promises polynomial time solutions for some SDA problems with large number of inputs while determining the class of problems which can be efficiently solved is an open future issue. The open issues to be solved for realizing QPC prototype as an alternative QC system are discussed in Section VIII. QPC method promises further studies for experimental verification and mathematical modeling of the set of problems that can be solved, i.e., determining the computational complexity class of problems solvable in polynomial time such as a group of NP-hard SDA problems or improving NP-intermediate (NPI) problems solvable with traditional QC algorithms [16].

The remainder of the paper is organized as follows. In Sections II and III, the physical set-up and the model of QPC are presented based on Feynman path integral formalism. Then, in Section IV, fundamental formulation of the computational power is modeled while in Section V, solutions for HSPs and SDA problems are presented. In Section VI, effects of exotic paths are modeled while in Section VII, numerical simulations are performed. Finally, in Sections VIII and IX, the open issues and conclusions are presented, respectively.

II. SYSTEM ARCHITECTURE

Assume that there are $N-1$ planes of slits in front of a particle source such as electrons or neutrons, and the interference pattern behind the last plane, i.e., plane with the index $N-1$, is observed by a detector array or screen denoted by the plane index N as shown in Fig. 1(a). The particles are assumed to perform free space propagation. The jth plane has $S_{j,T} \equiv 2\,S_j + 1$ number of slits where the central positions and the widths of the slits are given by $X_{j,i}$ and $D_{j,i}$, respectively, where $j \in [1, N-1]$ and $i \in [-S_j, S_j]$, and the set of ordered slit positions on jth plane is denoted by the column vector $\vec{X}_j$. The row vectors are represented with the transpose operation, i.e., $(.)^T$. In the following sections, the widths of the slits are chosen uniformly along each plane but differently among the planes. The whole set of the slit positions on $N-1$ parallel planes are denoted by $\mathbf{X}_{N-1}$. The distance between ith and jth planes is given by $L_{i,j}$ where the

distance from the particle emission source to the first plane and from $(N-1)$th plane to the detection plane are given by $L_{0,1}$ and $L_{N-1,N}$, respectively. The behavior of the particle is assumed to be classical in z-axis with the velocity given by v_z while the quantum superposition interference is assumed to be observed in x-axis as a one dimensional model. The model can be easily extended to the two dimensional (2D) systems. The distance between the planes is assumed to be much larger compared with the slit widths and the slit positions in x-axis.

The time duration for the particle to travel between $(j-1)$th and jth planes is assumed to be $t_{j-1,j} = v_z / L_{j-1,j}$ for $j \in [1, N]$ where $t_{N-1,N}$ denotes the observation time after the particle passes through $(N-1)$th plane. The position in x-axis on jth plane is denoted by x_j while the wave functions of a specific nth path and superposition of all the previous paths on jth plane are denoted by $\Psi_{n,j}(x_j)$ and $\Psi_j(x_j)$, respectively. Inter-plane distance and inter-plane duration vectors are represented by $\vec{L} = [L_{0,1} \ldots L_{N-1,N}]$ and $\vec{t} = [t_{0,1} \ldots t_{N-1,N}]$, respectively. The paths of the particle are assumed to be indexed by n for $n \in [0, N_p - 1]$ as shown in Fig. 1(b) where $N_p = \prod_{j=1}^{N-1} S_{j,T}$ and $Path_n \equiv \{s_{n,1}, s_{n,2}, \ldots s_{n,N-1}; s_{n,j} \in [-S_j, S_j]\}$. Therefore, the slit position for nth path on jth plane is given by $X_{n,s_{n,j}}$. The number of paths given by N_p can be significantly large for even a small number of planes and slits, e.g., reaching $> 10^{12}$ distinct paths interfering on the detector plane for $N-1 = 12$ and $S_j = 5$ for $j \in [1, 12]$. There are some assumptions making the model more clarified:

- The plane material is assumed to be absorbing without particle reflection between the slits making calculation much more complicated as shown in Fig. 1(d) while exotic paths are taken into account as shown in Fig. 1(c). The particle interfering on the detector plane is the one passing freely through the slits with free space propagation.

- Calculation of the inter-plane durations by $t_{j-1,j} = v_z / L_{j-1,j}$ is highly accurate due to $L_{j-1,j} \gg D_{j-1,i}, X_{j-1,i}$ for $j \in [2, N-1]$ and $i \in [-S_j, S_j]$, and setting $L_{01}, L_{N-1,N} \gg L_{j-1,j}$ in simulation studies (verified by simulation studies for the effect on the detector plane intensity) such that the quantum effects are emphasized in x-axis.

- Non-relativistic modeling of the particle behavior is assumed since the gravitational effects are neglected in the proposed dimensions.

- As a proof of concept, the source is a single Gaussian wave function while the slits are modeled as having Gaussian widths with Feynman path integral approach [1].

Next, Feynman path integral formalism is utilized to model the interference on the detector screen.

III. MULTI-PLANE AND MULTI-SLIT INTERFERENCE MODELING

The wave function on the detector plane for a specific path index n denoted by $\Psi_{n,N}(x)$ is calculated by using Feynman path integrals by using the free particle kernels [1]. Assume that $K(x_1, t_1; x_0, t_0) = \sqrt{m / (2\pi i \hbar \Delta t)} \exp(i m \Delta x^2 / (2 \hbar \Delta t))$ denotes the free particle kernel for the paths between the time-position values (t_0, x_0) and (t_1, x_1) where $\Delta t = t_1 - t_0$ and $\Delta x = x_1 - x_0$, m is the free particle mass and $\hbar$ is the Planck's constant. Assuming that x_j for $j \in [1, N-1]$ denotes the integration variable for the slit with the index $s_{n,j}$ and position $X_{j,s_{n,j}}$ in nth path and $\int_{\vec{x}} d\vec{x}$ denotes the integration with respect to the variables x_j for $j \in [0, N-1]$ between the limits $-\infty$ and ∞, then $\Psi_{n,N}(x)$ is given by the following:

$$
\begin{aligned}
\Psi_{n,N}(x) = \int_{\vec{x}} & K(x, t_N; x_{N-1}, t_{N-1}) \\
& \times G_{n,N-1}(x_{N-1} - X_{N-1,s_{n,N-1}}) \\
\times \prod_{j=1}^{N-2} & K(x_{j+1}, t_{j+1}; x_j, t_j) \, G_{n,j}(x_j - X_{j,s_{n,j}}) \\
& \times K(x_1, t_1; x_0, t_0) \, \Psi_0(x_0) \, d\vec{x}
\end{aligned}
\tag{1}
$$

where $t_j = t_0 + \sum_{k=1}^{j} t_{k-1,k}$ for $j \in [0, N]$, $G_{n,j}(x_j)$ denotes the effective function of the slit with the index $s_{n,j}$ on jth plane for nth path, e.g., rectangular or Gaussian slits as described in [1], and $\Psi_0(x_0)$ is the source wave function. The resulting integration is described in terms of linear canonical transforms (LCTs) providing a more intuitive description of the effects of interference on the final wave function for each path. LCT of a function $f(x)$ is defined as follows [17]:

$$
\begin{aligned}
LCT_{a,b,c,d}\{f(x)\} \equiv & e^{-i\frac{\pi}{4}} \sqrt{\eta} \\
\times \int_{-\infty}^{\infty} & e^{i\pi(\alpha x^2 - 2\eta x u + \gamma u^2)} f(u) du
\end{aligned}
\tag{2}
$$

where the LCT matrix is denoted by the following:

$$
\begin{bmatrix} a & b \\ c & d \end{bmatrix} = \begin{bmatrix} \frac{\gamma}{\eta} & \frac{1}{\eta} \\ \frac{\alpha\gamma - \eta^2}{\eta} & \frac{\alpha}{\eta} \end{bmatrix}
\tag{3}
$$

and $a d - b c = 1$ for a given set of parameters (α, γ, η). Then, it is easily shown that the evolution of $\Psi_0(x_0)$ in nth path is represented by the block diagram as shown in Fig. 2 where $LCT_{n,j}\{.\}$ denotes the LCT with the following transformation matrix:

$$
\begin{bmatrix} a_{n,j} & b_{n,j} \\ c_{n,j} & d_{n,j} \end{bmatrix} = \begin{bmatrix} 1 & \frac{2\pi\hbar t_{j,j+1}}{m} \\ 0 & 1 \end{bmatrix}
\tag{4}
$$

with the transformation parameters $\alpha = \gamma = \eta = m / (2\pi\hbar t_{j,j+1})$ for $j \in [0, N-1]$ not depending on the path index n due to the classical approximation in z-axis. It is also called as chirp or Fresnel transform in
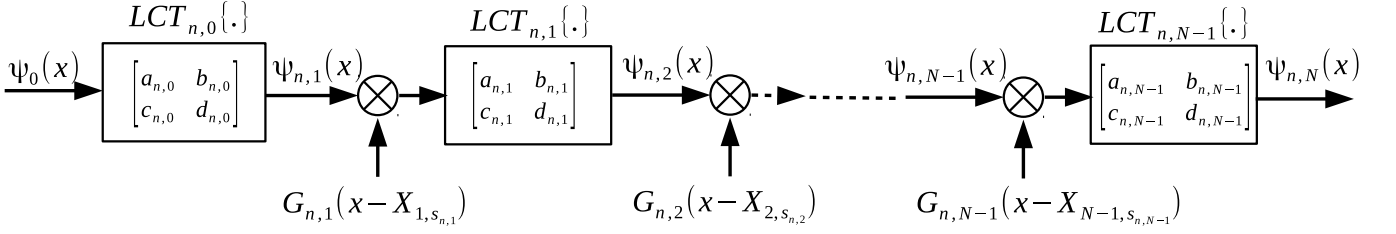
FIG. 2. The representation of evolution of the source wave function $\Psi_0(x)$ in nth path as consecutive operations of $LCT_{n,0}\{.\}$ followed by the operations of $LCT_{n,k}\{.\}$ and multiplication by the effective slit functions $G_{n,j}(x_j)$ for $j \in [1, N-1]$ resulting in the final wave function of $\Psi_{n,N}(x)$.

optical signaling literature [17]. The wave function on the boundary of each plane is denoted by $\Psi_{n,j}(x)$ for $j \in [1, N-1]$ while $\Psi_{n,N}(x)$ denotes the final wave function on the detector plane. Next, QPC method is presented where superposition interference is uniquely exploited for QC.

IV. QUANTUM PATH COMPUTING

The interfering wave function on the image plane is calculated based on Feynman path integrals and the result is transformed into a form to exploit quantum superposition for performing quantum computing tasks. Quantum wave pattern on screen is calculated by using Gaussian beams and slits with the forms of $G_{n,j}(x) = \exp(-x^2/(2\beta_j^2))$ with identical slits over each plane but with different effective slit widths $D_{j,i} \equiv 2\beta_j$ among the planes, and $\Psi_0(x) = \exp(-x^2/(2\sigma_0^2))/\sqrt{\sigma_0\sqrt{\pi}}$ [1, 7]. These assumptions can be replaced with different slit models without modification in the main idea of QPC but resulting into different functional forms of the path integrals. After integrating in (1) with Gaussian slits and Gaussian beam sources, the following wave function is obtained on jth plane:

$$\Psi_{n,j}(x) = \chi_0 \left(\prod_{k=1}^{j-1} \chi_{n,k} \right)$$
$$\times e^{(A_{j-1}+\imath B_{j-1})x^2 + (C_{n,j-1}+\imath D_{n,j-1})x} \quad (5)$$

where $j \in [1, N]$, x corresponds to the position in x-axis on jth plane and the iterative variables $\chi_{n,j}$, A_j, B_j, $C_{n,j}$ and $D_{n,j}$ are defined in Appendix A. Then, the resulting wave function $\Psi_{n,N}(x)$ is given by the following with the proof given in Appendix A:

$$\Psi_{n,N}(x) = \chi_0 \left(\prod_{j=1}^{N-1} \sqrt{\xi_j} \right)$$
$$\times \exp\left\{ \sum_{k=1}^{3} \vec{p_k}^T \left((\mathbf{M}_{1,k}\,\vec{x}_{n,N-1}) \odot (\mathbf{M}_{2,k}\,\vec{x}_{n,N-1}) \right) \right\}$$
$$\times e^{(A_{N-1}+\imath B_{N-1})x^2 + (\vec{c}_{N-1}^T + \imath \vec{d}_{N-1}^T)\vec{x}_{n,N-1}\,x} \quad (6)$$

where $\mathbf{M}_{1,1} = \mathbf{M}_{2,1} = \mathbf{I_{N-1}}$, $\mathbf{M}_{1,2} = \mathbf{M}_{2,2} = \mathbf{G}$, $\mathbf{M}_{1,3} = \mathbf{G}$, $\mathbf{M}_{2,3} = \mathbf{E}_1$, $\mathbf{I_k}$ is the identity matrix of size k, the complex valued matrices $\mathbf{G}$ and $\mathbf{E}_1$, the real valued column vectors $\vec{c}_{N-1}$, $\vec{d}_{N-1}$, the complex valued column vectors $\vec{p}_k$ for $k \in [1,3]$, real valued iterative variables A_j and B_j, and the complex valued iterative variable ξ_j are defined in Appendix A, and $\vec{x}_{n,k} = \begin{bmatrix} X_{1,s_{n,1}} & X_{2,s_{n,2}} & \dots & X_{k,s_{n,k}} \end{bmatrix}^T$. The superposition rule and Born's principle are utilized to find the relative intensity distribution on the display screen as follows:

$$I(x) = \left| \Psi_N(x) \right|^2 = \left| \sum_{n=0}^{N_p-1} \Psi_{n,N}(x) \right|^2$$
$$= \lambda\, e^{2A_{N-1}x^2} \left| \sum_{n=0}^{N_p-1} e^{r\{\vec{x}_n\}}\, e^{\vec{c}^T \vec{x}_n\, x}\, e^{\imath\, \vec{d}^T \vec{x}_n\, x} \right|^2 \quad (7)$$

where the subscript $N-1$ is dropped from the vectors to simplify the notation, e.g., $\vec{x}_n \equiv \vec{x}_{n,N-1}$, $\vec{c} \equiv \vec{c}_{N-1}$ and $\vec{d} \equiv \vec{d}_{N-1}$, $\lambda \propto |\chi_0 \prod_{j=1}^{N-1} \sqrt{\xi_j}|^2$ is some constant regarding the amount of intensity on the screen depending on the set-up and electron beam intensity, and $r\{\vec{x}_n\} \equiv \sum_{k=1}^{3} \vec{p_k}^T \left((\mathbf{M}_{1,k}\,\vec{x}_n) \odot (\mathbf{M}_{2,k}\,\vec{x}_n) \right)$. It can be easily shown that $r\{\vec{x}_n\}$ is equal to the following where the proof is given in Appendix B:

$$r\{\vec{x}_n\} = \vec{x}_n^T \mathbf{H}\, \vec{x}_n \quad (8)$$

where the matrix $\mathbf{H}$ is given by the following:

$$\mathbf{H} = \sum_{k=1}^{3} \mathbf{M}_{2,k}^T \operatorname{diag}\{\vec{p}_k\}\, \mathbf{M}_{1,k} \quad (9)$$

where $\operatorname{diag}\{\vec{y}\}$ is the operator creating a diagonal matrix with the diagonal elements composed of the vector $\vec{y}$. Then, assuming that the intensity distribution normalized by $1/\lambda$ is denoted by $I_{norm}(x)$, the resulting pattern measured on the screen depending on the resolution of the measurement apparatus is given by the following:

$$I_{norm}(x) = e^{2A_{N-1}x^2}$$
$$\times \left| \sum_{n=0}^{N_p-1} e^{\vec{x}_n^T \mathbf{H_R}\vec{x}_n}\, e^{\imath\, \vec{x}_n^T \mathbf{H_I}\vec{x}_n}\, e^{\vec{c}^T \vec{x}_n\, x}\, e^{\imath\, \vec{d}^T \vec{x}_n\, x} \right|^2 \quad (10)$$

where $\mathbf{H} = \mathbf{H_R} + \imath\,\mathbf{H_I}$ is composed of correlated real $\mathbf{H_R}$ and imaginary parts $\mathbf{H_I}$ extracted from (9). This is the main equation where the computational power of the QPC resides. The combined design of $\vec{x}_n$, $\mathbf{H}$, $\vec{c}$, $\vec{d}$ and A_{N-1} by choosing specific set of x-axis samples promises a solution to a significant number of optimization problems including huge memory and time complexities with significantly large N_p. The quantum superposition in the measurement provides information about the collective behavior of $\mathbf{H}$, $\vec{c}$ and $\vec{d}$ for exponentially large number of sample vectors $\vec{x}_n$ with a summation over them. Assuming that $N_p = (2\,S_0 + 1)^{N-1}$ where $S_j = S_0$ for $j \in [1, N-1]$, then a single measurement at the sample position x provides the information about the collective result of $(2\,S_0 + 1)^{N-1} \times (N-1)$ multiplications performing $\vec{d}^T \vec{x}_n$ for $n \in [0, N_p - 1]$. Similar to the traditional quantum algorithms exploiting superposition, e.g., period finding, Grover search or factoring or more generally denoted as *hidden subgroup problem (HSP)* [16], a clever way is necessary to best utilize the QPC power of (10) as provided in the next section.

The number of degrees of freedom to tailor the matrices for a general QPC set-up is $\sum_{j=1}^{N-1} S_{j,T} + N + (N-1) + 1 = \sum_{j=1}^{N-1} S_{j,T} + 2\,N$ where the first summation term is due to distinct positions of slits in each plane, the term N due to the number of inter-plane distances, the term $N-1$ due to different slit widths β_j for $j \in [1, N-1]$ and the last term due to σ_0. In the following sections, a specific QPC set-up refers to the tuned parameters of $\vec{\beta}$, $\vec{L}$, σ_0 and T_s for the specific grid $\mathbf{X}_{N-1}$ forming the vectors $\vec{x}_n$ for $n \in [0, N_p - 1]$ and the vector $\vec{d}$ defining the number theoretic problem where T_s refers to the sampling period on the detector plane. Next, QPC framework is utilized to solve HSP for periodicity of $e^{\imath\,2\,\pi\,\vec{d}^T \vec{x}}$ with respect to $\vec{x}$ or SDA problem for the set of real numbers which are $(2\,\pi)^{-1}\,T_s$ scaled versions of $\vec{d}^T \vec{x}_n$ for $n \in [0, N_p - 1]$.

V. HIDDEN SUBGROUPS FOR NON-UNIFORM RECIPROCAL INTEGER LATTICES

Traditional QC algorithms exploit the superposition qubit state generated with quantum Hadamard transforms applied on two registers initially at $|\mathbf{0}\rangle\,|\mathbf{0}\rangle$ and functional evolution with controlled unitary transforms U in black boxes for a given periodic function $f(x) = f(x + r)$ [16]. The QPC equation in (10) allows to find the periodicities in $e^{\imath\,2\,\pi\,\vec{d}^T \vec{x}}$ as a complex problem for arbitrary sets of $\mathbf{X}_{N-1}$ and $\vec{d}$ as defined in the following problem definitions and Table I. The continuous intensity is renormalized and sampled to extract periodicities by defining $\widetilde{I}[k] \equiv I_{norm}[k]\,e^{-2\,A_{N-1}\,(k\,T_s)^2}$ as follows:

$$\widetilde{I}[k] \equiv \sum_{n=0}^{N_p-1} e^{\vec{x}_n^T\,(\mathbf{H_R})\,\vec{x}_n}\,e^{\vec{c}^T \vec{x}_n\,k\,T_s}\,e^{\imath\,\Theta[n,k]} \qquad (11)$$

where the measurement location x is represented in terms of the samples $k\,T_s$ for integer indices $k \in [-\infty, \infty]$ and the sampling period T_s, and $\Theta[n,k]$ is as follows:

$$\Theta[n,k] = \vec{x}_n^T\,\mathbf{H_I}\,\vec{x}_n + \vec{d}^T \vec{x}_n\,k\,T_s \qquad (12)$$

The analogy between the traditional QC period finding (the algorithm in Section 5.4.1 in [16]) and QPC period finding is shown in Table I which is explained in detail after defining the following computational problems:

Problem 1 *Periodicity Detection and Reciprocal Non-uniform Lattice: Find the minimum integer $\widetilde{k} \in \mathbb{Z}^+$ scaling a given $N-1$ dimensional real vector $\vec{d}$ for a given **non-uniform lattice** denoted by $\mathbf{X}_{N-1}^s$ (scaled with respect to $\mathbf{X}_{N-1}$) resulting in a **reciprocal integer lattice** denoted by Λ by minimizing the error term ϵ_n for $n \in [0, N_p - 1]$ in a defined average sense such that $\Lambda \equiv \{\widetilde{k}\,\vec{d}^T \vec{x}_n^s + \epsilon_n \in \mathbb{Z};\ \forall\,\vec{x}_n^s,\ n \in [0, N_p - 1]\}$ where the non-uniform lattice $\mathbf{X}_{N-1}^s$ formed of a set of real vectors $\vec{x}_n^s$ is defined as follows:*

$$\vec{x}_n^s = (2\,\pi)^{-1}\,T_s\,[\,\vec{x}_n(1)\ldots\vec{x}_n(N-1)\,]$$
$$with\ \ \vec{x}_n(j) \in \{X_{j,-S_j},\ \ldots,\ X_{j,S_j}\}$$
$$s.t.\ \ X_{j,i} - X_{j,i+1} > 2\,\alpha\,\beta_j;\ \ N \geq 2;\ \ \alpha \geq 1$$
$$where\ \ n \in [0, N_p - 1];\ j \in [1, N-1];\ i \in [-S_j, S_j - 1]$$
$$S_j,\ N \in \mathbb{Z}^+;\ \beta_j,\ T_s,\ \alpha \in \mathbb{R}^+;\ X_{j,i} \in \mathbb{R}$$
$$(13)$$

where $N_p \equiv \prod_{j=1}^{N-1}(2\,S_j + 1)$, and $\mathbb{Z}$, $\mathbb{Z}^+$, $\mathbb{R}$ and $\mathbb{R}^+$ denote the sets of integers, positive integers, real values and the positive real values, respectively.

The optimization problem defined in Problem 1 requests defining a set of integers scaling either $\vec{d}$ or $\mathbf{X}_{N-1}^s$ such that inner product of $\vec{d}$ with all vectors in $\mathbf{X}_{N-1}^s$ results in values very close to integers with errors given by ϵ_n. The condition $X_{j,i} - X_{j,i+1} > 2\,\alpha\,\beta_j$ satisfies that the central positions of two slits are separated by the distance at least as much as the summation of their half widths where increasing α results in better physical design to satisfy Gaussian slit properties. The other conditions are definitions of parameters of the physical set-up described in Sections III and IV. Similarly, a parallel problem, i.e., SDA problem with NP-hard complexity modeled in [18], is defined as follows:

Problem 2 *Simultaneous Diophantine Approximation: Decide the existence and find the minimum integer $\widetilde{k} \in \mathbb{Z}^+$ where $\widetilde{k} \leq K_{pre}$ for some predefined $K_{pre} \in \mathbb{Z}^+$ such that it is the SDA solution for the set of real numbers in the set $S_b = \{b_0,\ b_1,\ \ldots,\ b_{N_p-1}\}$ satisfying the relation $|\widetilde{k}\,b[n] - k_n| < \epsilon$ for $n \in [0, N_p - 1]$ and for some $k_n \in \mathbb{Z}$ specific to each n with the common denominator $\widetilde{k}$ where $b[n] \equiv \vec{d}^T \vec{x}_n^s$ and ϵ is the bound.*

The first problem has an exponential complexity with respect to N, i.e., requiring the inner product multiplications for $\prod_{j=1}^{N-1} S_{j,T}$ different $\vec{x}_n^s$ values and more difficultly rationalizing the resulting values. The reciprocal

TABLE I. The analogy between QC and QPC period finding algorithms

Steps	QC Period Finding Algorithm [16]		QPC Period Finding Algorithm	
	Procedure	♯ Ops.	Procedure	♯ Ops.
0	a. The function $f(x)$ b. x is integer, producing single bit output c. Periodic for $0 < r < 2^L$ integer: $f(x) = f(x+r)$ d. The black box performing $U\|x\rangle\|y\rangle = \|x\rangle\|y \oplus f(x)\rangle$	0	a. The function $f(\vec{\boldsymbol{x}}) = e^{\imath\,2\,\pi\,\vec{\boldsymbol{d}}^T\,\vec{\boldsymbol{x}}}$, $\vec{\boldsymbol{x}}$ and $\vec{\boldsymbol{d}}$ are real vectors b. The basis periodicity sets defined as $S_a : \{\vec{\boldsymbol{r}}_a = \sum_{n=0}^{N_p-1} a_n \vec{\boldsymbol{x}}_n^s, a_n \in \mathbb{Z}, n \in [0, N_p-1]\}$ for $\vec{\boldsymbol{x}}_n^s \in \mathbf{X_{N-1}^s}$ c. $f(\vec{\boldsymbol{x}}) = f(\vec{\boldsymbol{x}} + \widetilde{k}\,\vec{\boldsymbol{r}}_a)$ with the sets $S_{\widetilde{k}} : \{\widetilde{k}\,\vec{\boldsymbol{r}}_a, \vec{\boldsymbol{r}_a} \in S_a\}$ d. The sensor plane counting the superposition intensity defined as $I(x) \equiv \left|\sum_{n=0}^{N_p-1} \Psi_{n,N}(x)\right|^2$ at the sample locations x	0
1	Initial state: $\|\mathbf{0}\rangle\|\mathbf{0}\rangle$	0	$\|\Psi_0\rangle$, $\Psi_0(x)$ formed as a simple Gaussian electron beam	0
2	Superposition: $\frac{1}{\sqrt{2^t}} \sum_0^{2^t-1} \|\mathbf{x}\rangle\|\mathbf{0}\rangle$	0	N_p paths to reach the detector with $\vec{\boldsymbol{x}}_n^s$ for $n \in [0, N_p - 1]$	0
3	Black box U: $\frac{1}{\sqrt{2^t}} \sum_0^{2^t-1} \|\mathbf{x}\rangle\|f(\mathbf{x})\rangle$	1	The set-up of $\mathbf{X}_{N-1}^s$, $\vec{\boldsymbol{\beta}}$, $\vec{\boldsymbol{L}}$ and σ_0: $\Psi_N(x) = \sum_{n=0}^{N_p-1} \Psi_{n,N}(x)$	1
4	$IQFT$ on the first register: $\frac{1}{\sqrt{r}} \sum_0^{r-1} \left\|\widetilde{l/r}\right\rangle \left\|\widehat{f}(l)\right\rangle$	$O(L^2)$	$IFFT_M$ at p with the $IFFT$ size M: $\sum_{h=0}^{\widetilde{k}-1} \Gamma_M[\frac{p}{M}, \frac{h}{k}]$	$O(M\log M)$
5	Measure first register: $\widetilde{l/r}$	0	Check the inverse FFT (IFFT) at a set of $p \in [0, M-1]$ values for $M \geq \widetilde{k}$ to estimate $h/\widetilde{k}$ for $h \in [0, \widetilde{k}-1]$	0
6	Continued fractions: r	$O(L^3)$	Unbiased estimation converging with increasing number of samples at varying p values	Polynomial complexity

lattices are well defined for Bravais lattices where the crystal structure is defined by a transformation vector. On the other hand, quasicrystals or crystals with non-uniform set of grid points are more difficult to analyze due to the lack of the strict order but rather repeating patterns [19]. In the current case, the lattice $\mathbf{X}_{N-1}^s$ has not any assumption except that it is the intersection of $N-1$ different sets of $(N-2)$ dimensional planes where the number of planes in each set $j \in [1, N-1]$ is equal to $S_{j,T}$ and the planes are separated in a single dimension denoted with the position x_j without any defined periodicity or pattern.

The equivalent second problem is NP-hard as discussed in [18] and it is assumed that the inner product set of $\vec{d}^T \vec{\boldsymbol{x}}_n^s$ for $n \in [0, N_p - 1]$ achieves the desired set of real numbers $b[n]$ by tuning the physical system set-up parameters in the QPC solution. The transformation mapping an arbitrary SDA problem to the physical set-up parameters is left as a future work to be achieved based on the fundamental model in this article.

Problems 1 and 2 are solved with a polynomial complexity solution by utilizing (10-12) in combination with a set of measurements on at $x = k\,T_s$ as shown in the next sections. The steps of the proposed QPC algorithm are described as follows while the analogy with traditional QC period finding is shown in Table I:

0. Real vector $\vec{d}$ and real grid $\mathbf{X_{N-1}}$ with elements $\vec{\boldsymbol{x}}_n$ for $n \in [0, N_p - 1]$ are given where $\vec{\boldsymbol{x}}_n \equiv \left[X_{1,s_{n,1}}\, X_{2,s_{n,2}}\, \ldots\, X_{k,s_{n,N-1}}\right]^T$ and $\mathbf{X_{N-1}}$ is composed of the positions $X_{j,i}$ for $j \in [1, N-1]$ and

$i \in [-S_j, S_j]$. The function $f(\vec{\boldsymbol{x}}) = e^{\imath\,2\,\pi\,\vec{\boldsymbol{d}}^T\,\vec{\boldsymbol{x}}}$ has periodicity with respect to $\vec{\boldsymbol{x}}$ with the unknown period $\widetilde{k}$ and the given basis sets $S_a : \{\vec{\boldsymbol{r}}_a = \sum_{n=0}^{N_p-1} a_n \vec{\boldsymbol{x}}_n^s, a_n \in \mathbb{Z}, n \in [0, N_p - 1]\}$ while periodicity vector is given by $\widetilde{k} \sum_{n=0}^{N_p-1} a_n \vec{\boldsymbol{x}}_n^s$ for any $a_n \in \mathbb{Z}$ and $n \in [0, N_p - 1]$, and the target is to find $\widetilde{k}$ where $\vec{\boldsymbol{x}}_n^s \equiv (2\,\pi)^{-1}\,T_s\,\vec{\boldsymbol{x}}_n$. The black box is formed of QPC set-up with the ability to measure superposition intensity.

1. Initial state is set up by designing the wave function of the particle source.

2. The superposition is due to QPC set-up combining N_p different paths on the screen.

3. Black box is the QPC set-up with specially designed parameters providing $\vec{\boldsymbol{x}}_n$ in the grid $\mathbf{X_{N-1}}$ and the vector $\vec{d}$ while related parameters $\vec{c}$, $\mathbf{H}$, and the set-up parameters $\vec{\boldsymbol{\beta}}$, $\vec{\boldsymbol{L}}$, σ_0 and T_s to be optimally designed for the best estimation of $\widetilde{k}$.

4. A set of $M \geq \widetilde{k}$ samples are taken on the detector plane and IFFT operation with the output time index p results in information about $p/\widetilde{k}$ and $h/\widetilde{k}$ for $h \in [0, \widetilde{k} - 1]$ where $\Gamma_M[\frac{p}{M}, \frac{h}{k}]$ is in (18).

5. The number of samples at varying p values is increased until $\widetilde{k}$ for a converging and unbiased estimation of $\widetilde{k}$.

6. The estimation problem can be set as a parameter estimation problem for the set of damped sinusoids with diverging coefficients or the estimation can be made easier if the set-up satisfies some special properties as described in the following sections. Traditional period finding algorithms with polynomial time solutions are utilized to best estimate $\widetilde{k}$, i.e., $O(M \log M)$ complexity for FFT based solutions in frequency estimation of damped sinusoids [20].

IFFT operation with the number of samples M described in Step-4 is given as follows by using (11). Define the following discrete functions of n as $g_1[n] \equiv \vec{c}^T \vec{x}_n T_s$, $g_2[n] \equiv \vec{d}^T \vec{x}_n T_s$ and $g_3[n] \equiv e^{\vec{x}_n^T \mathbf{H} \vec{x}_n}$. Since $\vec{d}$ and $(2\pi)^{-1} T_s \vec{x}_n$ form an integer lattice for $n \in [0, N_p - 1]$ with the integer period $\widetilde{k}$, the expression $e^{\imath g_2[n] k}$ is simplified by $e^{\imath \widetilde{G}_2[n] 2\pi k / \widetilde{k}}$ due to periodicity with $\widetilde{k}$ where $\widetilde{G}_2[n]$ is a function mapping the interval $[0, N_p - 1]$ into an integer between $[0, \widetilde{k} - 1]$ depending on relation between $\vec{d}$ and $\mathbf{X}_{N-1}^s$. Then, if $IFFT\{Y\}[p]$ denotes IFFT of some discrete function $Y[k]$ at the time index p, IFFT with the size M by utilizing $k \in [0, M-1]$ results in the following:

$$IFFT_M\{\widetilde{I}\}[p] \equiv \frac{1}{\sqrt{M}} \sum_{k=0}^{M-1} \sum_{n=0}^{N_p-1} \sum_{l=0}^{N_p-1} g_3[n] g_3^*[l]$$
$$\times e^{(g_1[n] + g_1[l])k} e^{-\frac{\imath 2\pi k(\widetilde{G}_2[l] - \widetilde{G}_2[n])}{\widetilde{k}}} e^{\frac{\imath 2\pi k p}{M}} \quad (14)$$

$$= \sum_{n=0}^{N_p-1} \sum_{l=0}^{N_p-1} \frac{1}{\sqrt{M}} A[n,l] \frac{1 - \gamma_{n,l,p}^M}{1 - \gamma_{n,l,p}} \quad (15)$$

where $\gamma_{n,l,p}$ is defined as follows:

$$\gamma_{n,l,p} \equiv e^{\alpha[n,l]} e^{-\frac{\imath 2\pi}{M \widetilde{k}}(\Delta G_2[n,l] M - p \widetilde{k})} \quad (16)$$

where the diverging coefficients are $\alpha[n,l] = g_1[n] + g_1[l]$, the amplitudes $A[n,l] = g_3[n] g_3^*[l]$ and the set of multiplying coefficients of $\omega_0 \equiv 2\pi / \widetilde{k}$ is $\Delta G_2[n,l] = \widetilde{G}_2[l] - \widetilde{G}_2[n] \in [-\widetilde{k} + 1, 2\widetilde{k} - 2]$. Dividing the set of $[n,l]$ pairs in $[0, N_p - 1] \times [0, N_p - 1]$ into $\widetilde{k}$ regions with the index $h \in [0, \widetilde{k} - 1]$ and denoted by R_h results in the following:

$$IFFT_M\{\widetilde{I}\}[p] = \sum_{h=0}^{\widetilde{k}-1} \Gamma_M[\frac{p}{M}, \frac{h}{\widetilde{k}}] \quad (17)$$

where $mod(\Delta G_2[n,l], \widetilde{k}) = h$ and $\Gamma_M[\frac{p}{M}, \frac{h}{\widetilde{k}}]$ is as follows:

$$\Gamma_M[\frac{p}{M}, \frac{h}{\widetilde{k}}] = \sum_{n,l \in R_h} \frac{1}{\sqrt{M}} A[n,l]$$
$$\times \frac{1 - e^{\alpha[n,l] M} e^{-\imath 2\pi \frac{h M}{\widetilde{k}}}}{1 - e^{\alpha[n,l]} e^{-\imath 2\pi (\frac{h}{\widetilde{k}} - \frac{p}{M})}} \quad (18)$$

Furthermore, if $M = \widetilde{k}$, the following is obtained:

$$\Gamma_{\widetilde{k}}[\frac{p}{\widetilde{k}}, \frac{h}{\widetilde{k}}] = \sum_{n,l \in R_h} \frac{1}{\sqrt{\widetilde{k}}} A[n,l] \frac{1 - e^{\alpha[n,l] \widetilde{k}}}{1 - e^{\alpha[n,l]} e^{-\frac{\imath 2\pi}{\widetilde{k}}(h-p)}} \quad (19)$$

Then, if novel mathematical tools are designed utilizing $g_3[n]$ and $g_1[n]$ for computationally efficient estimation of $\widetilde{k}$, each sample point on the detector plane increases the estimation accuracy. Similar to the Bertocco algorithm for the single sinusoid case [20], it is observed that the exponentially increasing term in the numerator, i.e., $1 - e^{\alpha[n,l] M} e^{-\imath 2\pi \frac{h M}{\widetilde{k}}}$, results in fast phase oscillations for each $h \in [0, \widetilde{k} - 1]$ if $M < \widetilde{k}$. Various performance metrics are capable of detecting the high fluctuations, e.g., the following metric denoted by $R[M]$ is expected to be maximized around $M \approx \widetilde{k}$ as a polynomial complexity solution:

$$R[M] = \frac{\left| IFFT_M\{\widetilde{I}\}[0] \right|}{\frac{1}{M-1} \sum_{k=1}^{M} \left| IFFT_M\{\widetilde{I}\}[k] \right|} \quad (20)$$

where the high frequency components are averaged and their mean is compared with the zero frequency component. Then, by checking the points of $R[M]$ with respect to M, i.e., minimizing the high frequency components, allows roughly determining $\widetilde{k}$. On the other hand, the same periodicity is expected in $R[M]$ since at multiples of $\widetilde{k}$ the fluctuations are decreased. Next, the solution of the SDA problem with the QPC algorithm is proposed.

A. QPC Solution of the SDA Problem

The existence of $\widetilde{k} \leq K_{pre} \equiv M$ is checked by the existence of high fluctuation points in solution of the SDA problem defined in Problem 2. If there is no fluctuation, it is an indication of the absence of the bounded error ϵ such that the solution of the SDA problem does not exist for $k \leq M$. On the other hand, if there is a fluctuation, the set of fluctuating points are the best candidates for the SDA solution periods and it is necessary to test them and chose the best result. Moreover, the classical period finding algorithms with polynomial computational complexity are promising to find the periodicity if it exists [20]. However, formal mathematical proof for the decision of the SDA solution existence depending on more detailed models of $\vec{d}$ and $\mathbf{X_{N-1}}$ combined with $\mathbf{H}$ and $\vec{c}$ in (10) is left as a future work providing the metric for the fluctuation compared with the other values in the interval $1 \leq k \leq M$ to decide in favor of the existence of SDA solution. Furthermore, the set of SDA problems whose solutions are achieved by a specific QPC set-up should be mathematically modeled. In this article, example problems are simulated to show the simple and low complexity solution achieved by QPC as a proof of concept promising future system designs providing simple QPC solutions to specific sets of SDA problems.

Besides that, the polynomial solutions in SDA problem and the performance of the well defined Lenstra, Lenstra Jr., and Lovasz (LLL) algorithm for large number of inputs become highly prohibitive for $N_p \gg 1$ [18]. Assume that $||x||$ denotes the distance of the real number

x to the closest integer, the maximum of $||\widetilde{k}\,b[n]||$ for $n \in [0, N_p - 1]$ is smaller than some pre-defined ϵ_p and there is some pre-defined bound M with $M > \widetilde{k}$. Then, the LLL algorithm provides the estimation of $\widetilde{k}$ denoted by $\widehat{k}$ satisfying $1 < \widehat{k} < 2^{N_p/2}\,M$ and the maximum of the $||\widehat{k}\,b[n]||$ being smaller than $\sqrt{5\,N_p}\,2^{(N_p-1)/2}\,\epsilon_p$ with the number of operations depending on the input size [18]. Therefore, QPC algorithm not only promises a powerful approach as a candidate to solve the NP-hard problem for the decision of SDA solution existence and to find it but also improves the existing polynomial solution approaches requiring significant time steps and memory with a limited accuracy.

The error term for the SDA problem is defined as $\epsilon[n, M] \equiv min\{||M\,b[n]||\}$ for $n \in [0, N_p - 1]$. Then, $\overline{\epsilon}[M] \equiv (1/N_p)\sum_{n=0}^{N_p-1}\epsilon[n, M]$, $\epsilon_{max}[M] \equiv \max_n\{\epsilon[n, M]\}$ and $\epsilon_{min}[M] \equiv \min_n\{\epsilon[n, M]\}$ are good indicators for observing how M is close to the solution of the SDA problem, i.e., $\widetilde{k}$. If, in future studies based on the proposed model in this article, it becomes possible to provide a set-up for a special number theoretical problem by transforming it into a specific instance of approximating the solution of a SDA problem, then QPC system performs as a potential solver in polynomial time. However, the formal mathematical proof of modeling the family of the problems requires more analysis as a future work. On the other hand, although the accuracy of the digits of the SDA solution can be increased, there is potentially a limit to the accuracy due to combined effects of physical parameters including $\hbar$, π, and the inaccuracies in the coordinates of the physical locations, the distances of the planes, the widths of the slits and the plane thicknesses requiring further work on the highest accuracy of solving a specific SDA problem. Therefore, number theoretic problems should be converted to a model where minimizing $\overline{\epsilon}[M]$ should give an acceptable solution.

In the following chapters, in addition to IFFT based fundamental technique, two different approaches are introduced which may become more effective, i.e., utilizing special property of $g_3[n]$ and $g_1[n]$ resulting in periodicity in the local maximum of $\widetilde{I}[k]$ and considering the problem as fundamental frequency estimation for a sum of sinusoids. Estimation under heavy noise on the screen requires more advanced methods to extract periodicity. However, accuracy of IFFT method can be increased by diversity combining methods, e.g., increasing signal-to-noise ratio (SNR) in each sample point and realizing multiple experiments consecutively or in parallel.

B. Periodicity Detection in the Intensity Local Maximum

Assume that non-uniform lattice $\mathbf{X}_{N-1}^s$ and vector $\vec{d}$ are in a specific family providing the conditions defined in Theorem 1 as follows:

Theorem 1 *Assume that $N-1$ dimensional real vectors $\vec{c}$ and $\vec{d}$, and a non-uniform grid $\mathbf{X_{N-1}}$ satisfy the following while constructing intensity $\widetilde{I}[k]$ defined in (11):*

1. *$\vec{d}$ and $\mathbf{X_{N-1}^s}$ form an integer lattice with the integer period $\widetilde{k}$ and the sampling interval T_s allowing the simplification of the expression $e^{\imath\,g_2[n]\,k} = e^{\imath\,\vec{d}^T\,\vec{x}_n\,T_s\,k}$ by $e^{\imath\,\widetilde{G}_2[n]\,2\,\pi\,k\,/\,\widetilde{k}}$.*

2. *$|H[k, \widetilde{G}_2]| < |H[k, 0]|$ and $|H[k_1, 0]| > |H[k_2, 0]|$ where $0 \le k \le \widetilde{k}$, $k_2 < k_1 \le \widetilde{k}$, and $k, k_1, k_2 \in \mathbb{Z}$, and $H[k, o]$ is defined as follows:*

$$H[k, o] \equiv \sum_{n=0}^{N_p-1} g_3[n]e^{g_1[n]\,(\widetilde{k}-k)}e^{-\frac{\imath\,2\,\pi\,o[n]\,k}{\widetilde{k}}} \tag{21}$$

where $o[n] \in [0, \widetilde{k} - 1]$ refers to a specific mapping of $n \in [0, N_p - 1]$ with a discrete function $o(.)$ while $H[k, 0]$ refers to the case where $o(n) = 0$. Then, periodicity $\widetilde{k}$ is found by checking local maximums in intensity such that the following is satisfied for $k \in [0, \widetilde{k} - 1]$:

$$\widetilde{I}[\widetilde{k}] > \widetilde{I}[k] \tag{22}$$

The proof is provided in Appendix C.

Then, checking local maximum points $\widehat{k}$ with random samples of $\vec{d}^T\,\vec{x}_n\,\widehat{k}\,T_s\,/\,(2\,\pi)$ to verify for integer values determines the periodicity $\widetilde{k}$. However, performance can be increased by using various methods for frequency estimation of damped sinusoids as described in [20] such as FFT based methods as shown in the next section.

C. Periodicity Estimation for Diverging Sinusoids with Fundamental Frequency

The problem is considered as finding the fundamental frequency $\omega_0 = 2\,\pi\,/\,\widetilde{k}$ for the summation of complex sinusoidal signals if (11) is transformed into the following:

$$\widetilde{I}[k] = \sum_{n=0}^{N_p-1}\sum_{l=0}^{N_p-1} A[n, l]e^{\alpha[n,l]\,k}\,e^{-\imath\,\Delta G_2[n,l]\,\omega_0\,k} \tag{23}$$

The received intensity in noisy receiver case denoted by $I_{norm,n}[k]$ is modeled as follows:

$$I_{norm,n}[k] = I_{norm}[k] + n[k] \tag{24}$$

where $n[k]$ is the receiver noise modeled as Gaussian random process with independent samples and with the variance σ_k^2 which becomes proportional to $I_{norm}[k]$ if Poisson distribution is assumed for photonic applications. However, in simulation studies, various levels of SNR are simulated. Then, normalized intensity is found as follows where noise is amplified in normalization operation:

$$\widetilde{I}_n[k] = \widetilde{I}[k] + \widetilde{n}[k] \tag{25}$$

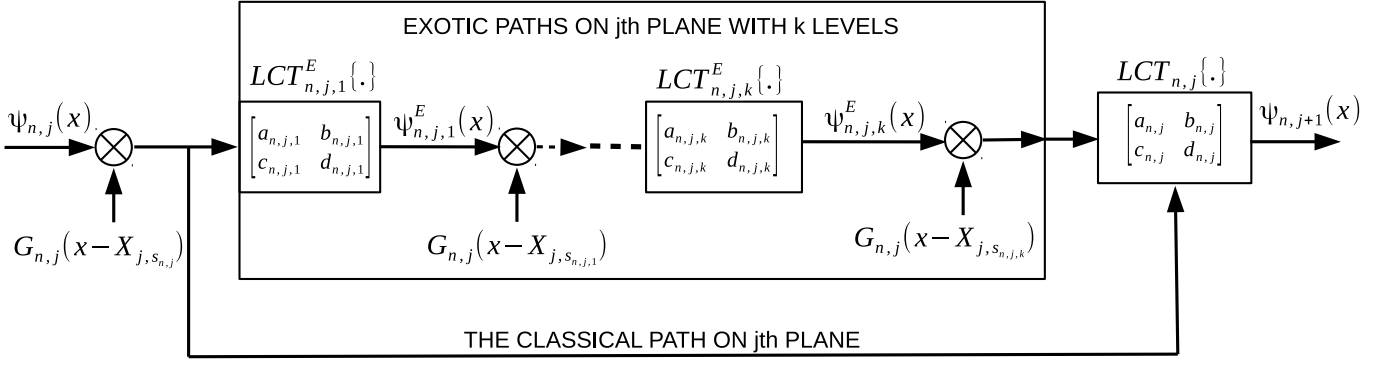FIG. 3. The representation of evolution of the source wave function $\Psi_{n,j}(x)$ on jth plane in nth path as consecutive operations of exotic movements $LCT^E_{n,j,i}\{.\}$ followed by multiplication of $G_{n,j}(x - X_{j,s_{n,j,i}})$ for $i \in [1,k]$ resulting in $\Psi_{n,j+1}(x)$.

where $\widetilde{n}[k] = e^{-2 A_{N-1} (k T_s)^2} n[k]$ with the variance $\widetilde{\sigma}^2[k] \equiv e^{-4 A_{N-1} (k T_s)^2} \sigma^2_k$ and $\sigma^2_k \leq \sigma^2_{max}$.

On the other hand, Cramer-Rao lower bound for the variance of the best estimate of $\widetilde{k}$ in noisy receiver case is provided in the following theorem which is useful to find performance of the best estimator:

Theorem 2 *The Cramer-Rao lower bound for the estimation of the periodicity in non-uniform integer lattice of the QPC set-up by using a set of intensity measurements on the screen in M different positions with sample points $k_p T_s$ for $p \in [0, M-1]$ is given as follows:*

$$CRB(\widetilde{k}) = \frac{(1 + \delta b(\widehat{k}) / \delta \widehat{k})^2}{\sum_{p=0}^{M-1} \left(\frac{1}{\widetilde{\sigma}[p]} \frac{\delta \widetilde{I}[k_p]}{\delta \widetilde{k}} \right)^2} \qquad (26)$$

where $b(\widehat{k}) \equiv E\{\widehat{k}\} - \widetilde{k}$ is the bias while the noise is assumed to have zero mean.

The proof is provided in Appendix D. Next, the effects of the exotic paths discussed in [7–10] are analyzed by extending previous formulations to include the effects of all possible exotic paths on the detector plane.

VI. EFFECTS OF EXOTIC PATHS

The evolved wave function is calculated by summing contributions from both classical and exotic paths by providing a complete formulation of the QPC set-up. A sample exotic path is shown in Fig. 1(c). Assume that the particle of nth path on jth plane makes k consecutive visits to slits in addition to the first slit or the entrance slit with the index $s_{n,j}$ and the position $X_{j,s_{n,j}}$ while the case with $k = 0$ corresponds to the classical path as shown in Fig. 3. Block diagram of evolution of the wave function in nth path is shown where the path is either a classical or an exotic path denoted with the same notations of $\Psi_{n,j}(x)$ and $\Psi_{n,j+1}(x)$ on jth and $j + 1$th planes, respectively. The wave function in the exotic path

after kth slit denoted by $\Psi^E_{n,j,k}(x)$ is explicitly provided in Appendix E for k bounded by some predetermined maximum number N_E. The parameters of $LCT^E_{n,j,k}\{.\}$ depend on the distance between the slits on jth plane defined as $\Delta^E_x(j,k) \equiv |X_{j,s_{n,j,k}} - X_{j,s_{n,j,k-1}}|$ where $X_{j,s_{n,j,k}}$ denotes the central position of kth visited slit and $k = 0$ case corresponds to the position of the first slit on jth plane, i.e., $X_{j,s_{n,j,0}} \equiv X_{j,s_{n,j}}$. Then, setting a maximum for N_E and finding all paths for $k \in [0, N_E]$ give an accurate result considering effects of all possible exotic paths.

The operator formalism for calculating Gouy phase in [7] is utilized to calculate time durations for the path distance $\Delta^E_x(j,k)$ with $t^E_{k-1,k}(j) \equiv \Delta^E_x(j,k) / \Delta^E_v(j) = m \Delta^E_x(j,k) / \Delta^E_p(j)$ where $\Delta^E_p(j) = \sqrt{\langle p^2 \rangle - \langle p \rangle^2}$ and $\langle p^a \rangle$ for $a \in [1,2]$ is defined as follows:

$$\langle p^a \rangle \equiv \int_{-\infty}^{\infty} \Psi^*_j(x) \left(\frac{\hbar}{\imath} \frac{\delta}{\delta x} \right)^a \Psi_j(x) \, dx \qquad (27)$$

where $\Psi_j(x)$ is the total wave function on jth plane as a superposition of all previous paths. The total number of different paths between jth and $(j+1)$th planes including exotic movements is denoted by $N_{e,j}$ which is calculated by the following formulation:

$$N_{e,j} = S_{j,T} \sum_{k=1}^{N_E} (S_{j,T} - 1)^k \qquad (28)$$

while the total number of all paths on ith plane for $i \in [1, N]$ is given by $N^E_{p,i} \equiv \prod_{j=1}^{i-1} N_{e,j}$. The total number of paths on the image plane is denoted by $N^E_{p,N}$ which is much larger compared with the case including only classical paths, i.e., N_p, and the total number of contributions and effects of the exotic paths are simulated in Section VII for the proposed sample problems. The first term $S_{j,T}$ shows different selections of the entrance slit while the remaining k different slit visitings occur in $(S_{j,T} - 1)^k$ permutations. Finally, summing the contributions for different k values until N_E results in (28). In the next section, numerical simulations are performed for two different SDA problems as a proof of concept.

TABLE II. QPC problems and simulation set-up parameters

ID	Property	Value
Sim_1	N, S_1, S_2	3, 2, 2
	$\vec{\boldsymbol{X}}_1^T$, $\vec{\boldsymbol{X}}_2^T$ (nm)	$[-6031.9 \quad -2960.6 \quad 110.7 \quad 3181.9 \quad 6253.2]$, $[-643.9 \quad -327.6 \quad -11.4 \quad 304.8 \quad 621.1]$
	$\vec{\boldsymbol{d}}^T$ (m^{-2})	$[-11825366721.5 \quad -114848915118.2]$
	$\vec{\boldsymbol{L}}^T$ (m), $\vec{\boldsymbol{\beta}}^T$ (nm)	$[1 \quad 400 \times 10^{-6} \quad 1]$, $[196.5 \quad 63.2]$
Sim_2	N, S_1, S_2	5, 1, 1
	$\vec{\boldsymbol{X}}_1^T$, $\vec{\boldsymbol{X}}_2^T$, $\vec{\boldsymbol{X}}_3^T$, $\vec{\boldsymbol{X}}_4^T$ (nm)	$[-4315.4 \quad 382.0 \quad 3513.6]$, $[-3610.0 \quad -570.0 \quad 950.0]$, $[-5887.7 \quad 506.0 \quad 2637.2]$, $[-2312.9 \quad -230.0 \quad 3935.9]$
	$\vec{\boldsymbol{d}}^T$ (m^{-2})	$[-36852879374.3 \quad -37760536805 \quad -25967723254.4 \quad -26078529374]$
	$\vec{\boldsymbol{L}}^T$ (m), $\vec{\boldsymbol{\beta}}^T$ (nm)	$[1 \quad 476.2 \times 10^{-6} \quad 222.2 \times 10^{-6} \quad 175.4 \times 10^{-6} \quad 1]$, $[191 \quad 190 \quad 230 \quad 230]$

TABLE III. The physical system parameters

Symbol	Value	Symbol	Value
m (kg)	$9.11\,10^{-31}$	$\hbar$ (J $\times$ s)	$1.05\,10^{-34}$
v_z (m/s)	$1.46\,10^7$	T_s (μm)	1
σ_0 (nm)	500		

TABLE IV. Path count on the slit and the sensor planes

	Sim_1		Sim_2			
	Plane-2	Sensor	Plane-2	Plane-3	Plane-4	Sensor
Classical	5	25	3	9	27	81
$N_E = 1$	25	625	9	81	729	6561
$N_E = 2$	105	11025	21	441	9261	194481
$N_E = 3$	425	180625	-	-	-	-

VII. NUMERICAL SIMULATIONS

The proof of concept QPC set-up is formed with classically tractable number of planes and with simplicity to verify the main features of the system design. Two different simulation experiments are achieved denoted by Sim_1 and Sim_2, respectively. In Sim_1, the real numbers $b[n]$ for $n \in [0, N_p - 1]$ are chosen in a specific pattern to allow for highly accurate solution to the SDA problem with significantly small error term. On the other hand, in Sim_2, SDA problem is defined for less accurate solution with an optimization approach finding the term minimizing the error in a large interval. The main system properties are shown in Table III where the fundamental physical parameters are chosen based on the electron beam based set-up verified for Gouy phase calculations in [7]. Two different QPC problems solved with

the system set-up are shown in Table II. The presented numbers are the rounded versions while the digits of precision are improved in MATLAB used for the simulations by utilizing variable precision arithmetic (vpa) to allow the contribution of path wave functions with significantly small amplitudes compared with the other paths.

A. Simulation-1: Accurate SDA Solution and Effects of the Exotic Paths

The number of slit planes is set to two with $N = 3$ and $S_i = 2$ for $i \in [1, 2]$ to observe the main mechanism of QPC by explicitly analyzing wave functions on each plane and clearly observing the effects of exotic paths. The total number of classical paths on the image plane is $N_p = 25$ while the number of all paths including exotic ones, i.e., $N_{p,N}^E$, for varying N_E is shown in Table IV for both Sim_1 and Sim_2. It is observed that as N_E increases, the number of exotic paths becomes significantly large making it computationally complex to find the final contribution on the image plane. It is observed that intensity converges as N_E increases and N_E is chosen as three and two for Sim_1 and Sim_2, respectively, with reduced computational problems.

The fractional numbers forming the SDA problem are shown in Fig. 4(a). They are chosen with a special pattern to satisfy an accurate SDA solution at $\widetilde{k} = 173$. The set-up parameters $\mathbf{X}_{N-1}^s$, $\vec{\boldsymbol{d}}$, $\vec{\boldsymbol{\beta}}$, $\vec{\boldsymbol{L}}$, σ_0 and T_s are designed to provide the desired set of real numbers. In Fig. 4(b), the error terms $\overline{\epsilon}[M]$, $\epsilon_{max}[M]$ and $\epsilon_{min}[M]$ are shown for Sim_1. The mean error term is smaller than 10^{-8} for $M = \widetilde{k} = 173$, which is assumed to be the SDA solution for the current problem with the accuracy of eight digits.

In Fig. 4(c), the normalized intensity $I_{norm}[k]$ is shown while $\widetilde{I}[k]$ and $|H[k,0]|^2$ are shown in Fig. 4(d) satisfying both the conditions in Theorem 1 such that $\widetilde{I}[k] > \widetilde{I}[0]$ and $\widetilde{I}[k] < |H[k,0]|^2$ for $k \leq \widetilde{k}$. Therefore, the value of $\widetilde{k}$ is easily extracted by checking either the periodicity or
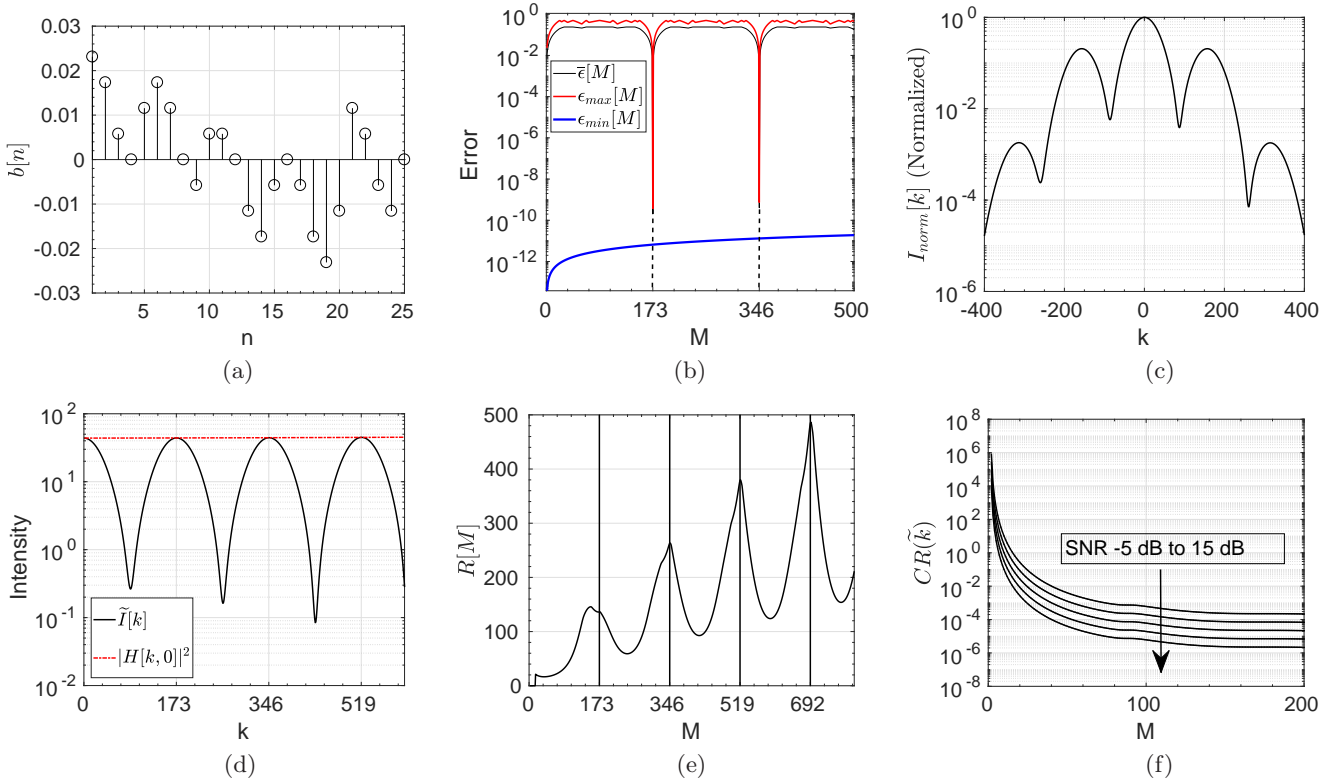
FIG. 4. (a) The distribution of the real numbers $b[n]$ for $n \in [0, N_p - 1]$ defining SDA problem of Sim_1, (b) error terms in SDA problem for varying M where the minimum error points are shown, (c) the normalized intensity and (d) $\widetilde{I}[k]$ on the detector plane, (e) $R[M]$ for varying M showing high fluctuations around multiples of $\widetilde{k}$, and (f) Cramer-Rao bound for estimating $\widetilde{k}$ for varying number of samples in $[0, M]$ and varying SNR in $[-5, 0, 5, 10, 15]$ dB.

the local maximum points of $\widetilde{I}[k]$. Besides that, $IFFT$ based method provides an accurate estimation of $\widetilde{k}$ as shown in Fig. 4(e). Fluctuations are more visible as M increases at multiples of 173 while the maximum points of $R[M]$ show periodicity of 173. On the other hand, CRB is shown for varying SNR in Fig. 4(f) with a low bound for the number of samples larger than a few tens. Therefore, periodicity estimation methods for damped sinusoids can be applied successfully such as [20].

The effects of exotic paths are simulated in Figs. 5 and 6. In Fig. 6, the intensity distribution on the planes of slits and the image plane are shown. Five different peaks are clearly observed on the second plane while interfering pattern is shown in the sensor plane and input wave function due to freely propagating Gaussian beam of electrons is shown on the first plane. The total normalized intensity distribution including the exotic paths for varying N_E is shown in Fig. 5(a). The main structure of the distribution is preserved while the effects for increasing N_E are attenuated as shown in Fig. 5(b) for the case of $N_E = 3$ where periodicity and value of $\widetilde{k}$ are still reliably extracted. The same observation is preserved in $R[M]$ for varying M in Fig. 5(c). The periodicity extraction by utilizing smaller number of samples results in small errors in the estimation of $\widetilde{k}$ while a converging estima-

tion is observed for the specific problem in Sim_1 as the number of samples is increased. However, utilizing values of $\widetilde{I}[k]$ for large k requires higher precision measurement instruments due to the significant attenuation at distant sample locations and potentially longer time to collect particles. Special tuning and design of QPC set-up can solve most of the problems in future architectures based on the fundamental idea of the QPC. Next, a more complicated SDA problem is solved by finding the optimum solution in a given interval minimizing error terms.

B. Simulation-2: SDA Problem for Larger Inputs

The number of slit planes is increased to $N - 1 = 4$ and $S_i = 1$ for $i \in [1, 4]$ to realize a QPC solution for a more complicated problem by approximating the SDA solution of 81 real numbers. The effect of exotic paths on the image plane is calculated for $N_E = 2$ since the effects of the exotic paths gradually decrease and it is enough to calculate for $N_E = 1$ and $N_E = 2$ to observe the change in received intensity waveform.

The set of fractional real numbers is shown in Fig. 7(a) while the error terms of the SDA problem are shown in Fig. 7(b) with an approximate solution of $M = \widetilde{k} = 111$
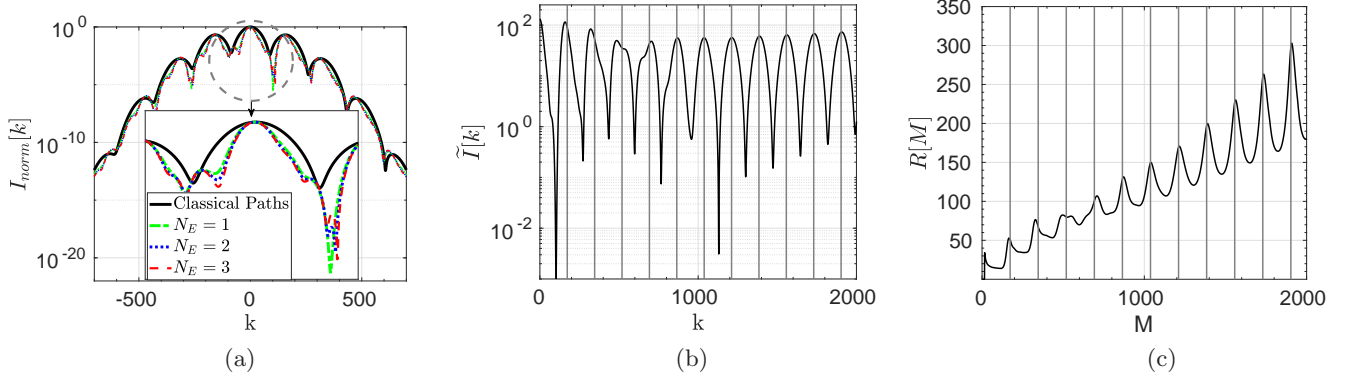
FIG. 5. (a) The normalized intensity distribution $I_{norm}[k]$ on the image plane by including effects of exotic paths and for varying N_E where the middle part shows zoomed intensity distribution at the center, (b) $\widetilde{I}[k]$ and (c) $R[M]$ for varying M for the case of $N_E = 3$ where the lines show multiples of $\widetilde{k} = 173$.
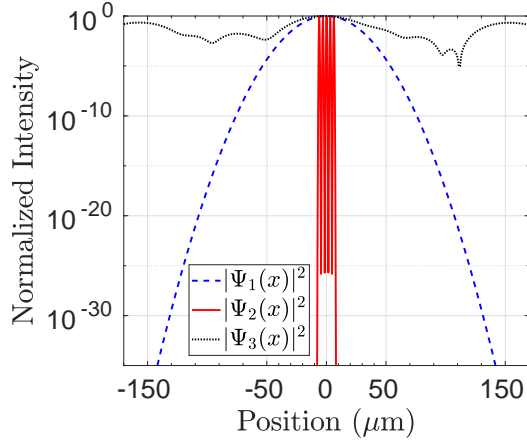

FIG. 6. The normalized intensity on the first, second and the image planes by including effects of exotic paths.

and with less accurate solutions at multiples of $\widetilde{k}$ minimizing the error terms. QPC algorithm is utilized to find these optimum points by also including the effects of the exotic paths. The normalized intensity and $\widetilde{I}[k]$ are shown in Figs. 7(c) and (d), respectively. The effects of exotic paths are more powerful at central part of the sensor plane while still keeping the envelope with periodicity $\approx \widetilde{k}$. Exotic path effects are smaller at non-central part of the sensor plane similar to the results of Sim_1. IFFT based method reliably finds multiples of $\widetilde{k} = 111$ by utilizing samples in interval $[0, 500]$ as shown in Fig. 7(e) with small errors around $\widetilde{k}$.

The model of the exact error in target periodicity is left as a future work. The significant result is that the computational power of QPC finds existence of periodicity and locates its position with a high accuracy in polynomial resource complexity. Similarly, normalized intensity attenuates very fast requiring higher precision sampling or diversity combining methods to improve SNR at distant

sampling locations. There is a trade-off between accuracy of periodicity extraction by utilizing distant sample locations and SNR of the particles.

VIII. DISCUSSION AND OPEN ISSUES

The QPC system design requires further efforts to be utilized as an alternative QC architecture based on the solution of the challenges and open issues listed as follows. The provided system design is valid for other particles including photons for optical QC setups or molecules for molecular computing architectures for next generation nanoscale communication and computing systems. The open issues are the following:

1. The formal mathematical proof for the decision of SDA solution existence, i.e., $\widetilde{k}$, depending on models of $\vec{c}$, $\vec{d}$, $\mathbf{H}$ and A_j for $j \in [0, N-1]$ with a metric for fluctuations compared with the other values in interval $1 \leq k \leq M$.

2. Defining the set of SDA problems formally whose solutions are achieved and not possible to achieve by a specific QPC set-up.

3. Providing the class of problems that QPC can solve exactly or provide an approximation to solutions of NP-hard or NP-intermediate problems [16].

4. Mapping from a target SDA problem to physical set-up parameters by utilizing highly complicated expressions of $\vec{c}$, $\vec{d}$, $\mathbf{H}$ and A_j for $j \in [0, N-1]$ described in Appendix A.

5. Designing the best classical frequency estimation method operating on samples of $\widetilde{I}$ by analyzing the state-of-the art polynomial solutions such as the ones reviewed in [20].
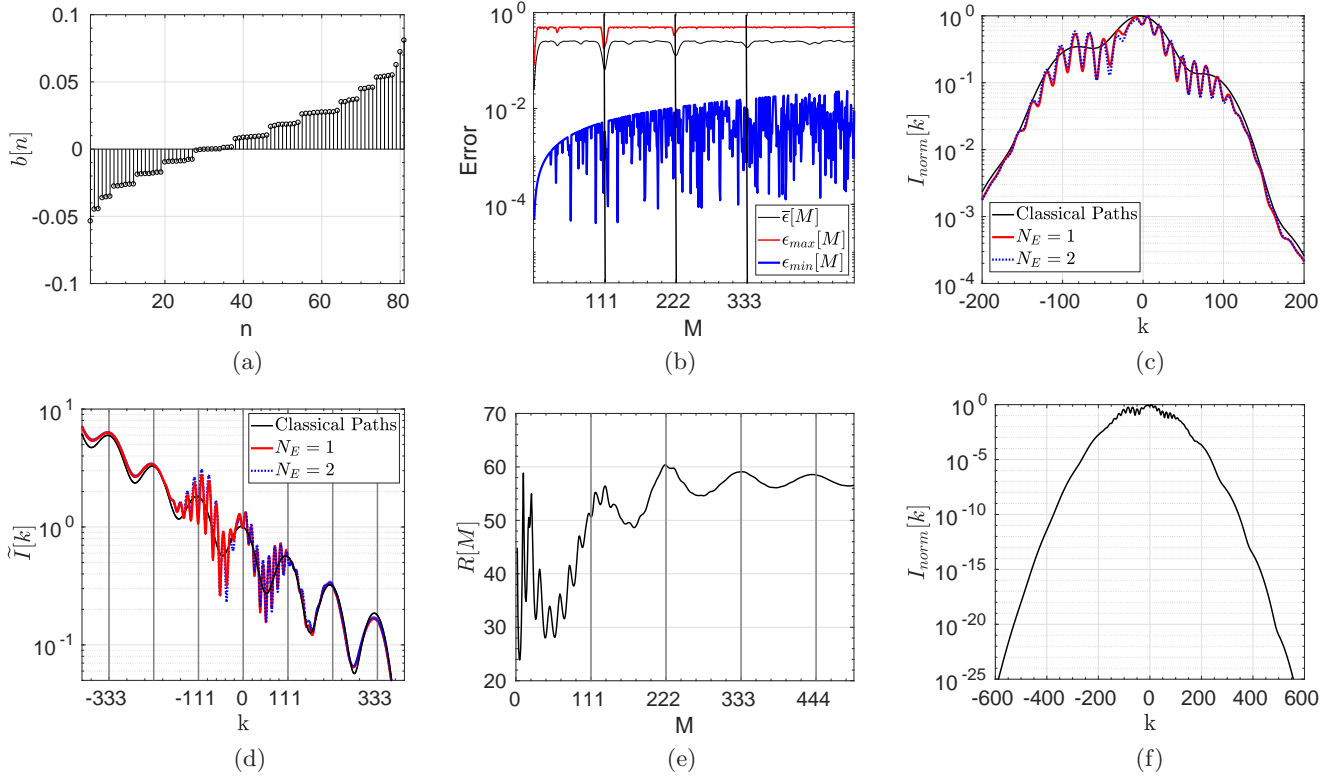
FIG. 7. (a) The set of 81 real numbers $b[n]$ defining the SDA problem of Sim_2, (b) error terms in SDA problem for varying M where the minimum error point is shown at $M = 111$, (c) normalized intensity $I_{norm}[n]$ and (d) $\widetilde{I}[k]$ on the detector plane for Sim_2 for both classical only paths and including the exotic contributions with $N_E = 1, 2$, (e) $R[M]$ for varying M for the case of $N_E = 2$, and (f) significant attenuation of $I_{norm}[n]$ at distant sample points.

6. Experimental verification of the proposed system set-up and extension for other particles including photons and molecules by providing easier system design and utilization in molecular and nanoscale computing architectures.

7. As the planes are getting closer, accuracy of assuming $t_{j,j+1}$ constant for all paths on jth plane decreases, and appears as an error term.

8. Gaussian slit approximation for particles should be verified experimentally and the width β_j for $j \in [1, N-1]$ should be determined experimentally by tuning the value for a fixed slit width giving the smallest error in periodicity estimation. The photonic implementations with significantly thin planes, e.g., graphene or similar 2D materials, are candidates to form perfect Gaussian slits.

IX. CONCLUSION

In this article, a simple and low complexity quantum computing architecture is presented by utilizing multi-plane and multi-slit quantum superposition interference and Feynman path integral formalism. The proposed system denoted by QPC achieves to find solutions to HSPs and provides theoretical framework promising solution steps for some set of NP-hard SDA problems. Simulation results provide polynomial time solutions to the specifically designed simple SDA problems. QPC system is a low complexity, low cost and simple QC architecture operating at the room temperature for finding polynomial solutions to some set of problems requiring exponentially complex time and memory resources. QPC is a competitive alternative to existing QC systems having significant challenges in terms of complexity and the performance.

Appendix A

The first integration is obtained with $\Psi_0(x) = \exp\big(-x^2 / (2\,\sigma_0^2)\big) / \sqrt{\sigma_0\sqrt{\pi}}$ with free propagation until the first slit plane resulting in the following parameters:

$$A_0 = -\frac{m^2\sigma_0^2}{2\,\hbar^2 t_{0,1}^2 \,+\, 2\,m^2\sigma_0^4} \tag{A1}$$

$$B_0 = \frac{\hbar\,m\,t_{0,1}}{2\,\hbar^2 t_{0,1}^2 \,+\, 2m^2\sigma_0^4} \tag{A2}$$

$$\chi_0 = \frac{1}{\pi^{1/4}} \sqrt{\frac{m\,\sigma_0}{m\,\sigma_0^2 \,+\, \imath\,\hbar\,t_{0,1}}} \tag{A3}$$

while $C_0 = D_0 = 0$. The second LCT results in the following signal coefficients:

$$A_1 = \frac{\beta_1^2 \, m^2 \, (2 \, A_0 \, \beta_1^2 - 1)}{2 \, \zeta_1} \tag{A4}$$

$$B_1 = \frac{2 \, B_0 \, \beta_1^4 \, m^2 + \hbar \, m \, t_{1,2} \, \varrho_1}{2 \, \zeta_1} \tag{A5}$$

$$C_{n,1} = \zeta_{1,c} \, X_{1,s_{n,1}} \tag{A6}$$

$$D_{n,1} = \zeta_{1,d} \, X_{1,s_{n,1}} \tag{A7}$$

$$\chi_{n,1} = e^{p_{1,1} \, X_{1,s_{n,1}}^2} \sqrt{\xi_1} \tag{A8}$$

where the following variables are defined:

$$p_{1,j} \equiv -\left(2 \, \hbar \, t_{j,j+1}(A_{j-1} + \imath B_{j-1}) + \imath m\right) / (2 \imath \varsigma_j)$$
$$\varsigma_j \equiv \beta_j^2 \, m + \hbar \, t_{j,j+1} \left(2 \, \beta_j^2 \, (B_{j-1} - \imath A_{j-1}) + \imath\right)$$
$$\xi_j \equiv \beta_j^2 m / \varsigma_j$$
$$\varrho_j \equiv 4 \, \beta_j^4 \, (A_{j-1}^2 + B_{j-1}^2) - 4 \, A_{j-1}\beta_j^2 + 1$$
$$\zeta_j \equiv 4 \, B_{j-1} \, \beta_j^4 \, \hbar \, m \, t_{j,j+1} + \beta_j^4 \, m^2 + \hbar^2 \, t_{j,j+1}^2 \, \varrho_j$$
$$\zeta_{j,c} \equiv \left(2 \, B_{j-1} \, \hbar \, m \, t_{j,j+1} \, \beta_j^2 + \beta_j^2 \, m^2\right) / \zeta_j$$
$$\zeta_{j,d} \equiv \hbar \, m \, t_{j,j+1} \left(2 \, A_{j-1} \, \beta_j^2 - 1\right) / \zeta_j$$

Then, from the third LCT until the final plane, i.e., for $j \in [2, N-1]$, the following iterations are obtained:

$$A_j = \frac{\beta_j^2 \, m^2 \, (2 \, A_{j-1} \, \beta_j^2 - 1)}{2 \, \zeta_j} \tag{A9}$$

$$B_j = \frac{2 \, B_{j-1} \, \beta_j^4 \, m^2 + \hbar \, m \, t_{j,j+1} \, \varrho_j}{2 \, \zeta_j} \tag{A10}$$

$$C_{n,j} = , \zeta_{j,c} \, X_{j,s_{n,j}} + p_{4,j} C_{n,j-1} + p_{5,j} \, D_{n,j-1} \tag{A11}$$

$$D_{n,j} = \zeta_{j,d} \, X_{j,s_{n,j}} - p_{5,j} C_{n,j-1} + p_{4,j} \, D_{n,j-1} \tag{A12}$$

$$\chi_{n,j} = \sqrt{\xi_j} \, e^{p_{1,j} \, X_{j,s_{n,j}}^2} \, e^{p_{2,j} \, (C_{n,j-1} + \imath D_{n,j-1})^2}$$
$$\times \, e^{p_{3,j} \, (C_{n,j-1} + \imath D_{n,j-1}) \, X_{j,s_{n,j}}} \tag{A13}$$

$$\chi_{T,j} = \chi_0 \prod_{k=1}^{j} \chi_{n,k} \tag{A14}$$

where the following variables are defined:

$$p_{2,j} \equiv -\frac{\beta_j^2 \, \hbar \, t_{j,j+1}}{2 \imath \varsigma_j} \tag{A15}$$

$$p_{3,j} \equiv -\frac{\hbar \, t_{j,j+1}}{\imath \varsigma_j} \tag{A16}$$

$$p_{4,j} \equiv \beta_j^2 \, \zeta_{j,c} \tag{A17}$$

$$p_{5,j} \equiv \frac{-2 \, \hbar \, t_{j,j+1}}{m} \, A_j \tag{A18}$$

Then, if (A11) and (A12) are converted into a vectorial iterative relation, and including the path index n in the notations of C_j and D_j, the following is satisfied:

$$\begin{bmatrix} C_{n,j} \\ D_{n,j} \end{bmatrix} = \begin{bmatrix} \zeta_{j,c} \\ \zeta_{j,d} \end{bmatrix} X_{j,s_{n,j}} + \begin{bmatrix} p_{4,j} & p_{5,j} \\ -p_{5,j} & p_{4,j} \end{bmatrix} \begin{bmatrix} C_{n,j-1} \\ D_{n,j-1} \end{bmatrix} \tag{A19}$$

Performing iterations result in $C_{n,N-1} = \vec{c}_{N-1}^T \vec{x}_{n,N-1}$ and $D_{n,N-1} = \vec{d}_{N-1}^T \vec{x}_{n,N-1}$ where jth element of the vector $\vec{x}_{n,N-1}$ of the length $N-1$ is defined as $X_{j,s_{n,j}}$, and the row vectors $\vec{c}_j^T$ and $\vec{d}_j^T$ are defined as follows:

$$\begin{bmatrix} \vec{c}_j^T \\ \vec{d}_j^T \end{bmatrix} \equiv \begin{bmatrix} \vec{v}_{0,j} & \vec{v}_{1,j} & \ldots & \vec{v}_{j-1,j} \end{bmatrix} \tag{A20}$$

and $\vec{v}_{k,j}$ for $k \in [0, j-1]$ to obtain $C_{n,j} = \vec{c}_j^T \vec{x}_{n,j}$ and $D_{n,j} = \vec{d}_j^T \vec{x}_{n,j}$ is given by the following:

$$\vec{v}_{k,j} = \left(\prod_{i=1}^{j-1-k} \begin{bmatrix} p_{4,j+1-i} & p_{5,j+1-i} \\ -p_{5,j+1-i} & p_{4,j+1-i} \end{bmatrix} \right) \begin{bmatrix} \zeta_{k+1,c} \\ \zeta_{k+1,d} \end{bmatrix} \tag{A21}$$

where matrix multiplication symbol $\prod_{i=1}^{k} \mathbf{H}_i$ denotes $\mathbf{H}_1 \, \mathbf{H}_2 \ldots \mathbf{H}_k$ for any matrix $\mathbf{H}_i$ for $i \in [1, k]$. Putting the resulting expressions of $C_{n,N-1}$ and $D_{n,N-1}$ into (A13) and (A14), the following is obtained:

$$\chi_{T,N-1} = \chi_0 \left(\prod_{j=1}^{N-1} \sqrt{\xi_j} \right) \left(\prod_{j=1}^{N-1} e^{p_{1,j} \, X_{j,s_{n,j}}^2} \right)$$
$$\times \left(\prod_{j=2}^{N-1} e^{p_{2,j} \, (\vec{c}_{j-1}^T \vec{x}_{n,j-1} + \imath \, \vec{d}_{j-1}^T \vec{x}_{n,j-1})^2} \right)$$
$$\times \left(\prod_{j=2}^{N-1} e^{p_{3,j} \, (\vec{c}_{j-1}^T \vec{x}_{n,j-1} + \imath \, \vec{d}_{j-1}^T \vec{x}_{n,j-1}) \, X_{j,s_{n,j}}} \right) \tag{A22}$$
$$= \chi_0 \left(\prod_{j=1}^{N-1} \sqrt{\xi_j} \right) e^{\vec{p}_1^T \, \vec{g}_{n,1}} \, e^{\vec{p}_2^T \, \vec{g}_{n,2}} \, e^{\vec{p}_3^T \, \vec{g}_{n,3}} \tag{A23}$$

where $\vec{p}_1^T \equiv [p_{1,1} \ldots p_{1,N-1}]$, $\vec{p}_2^T \equiv [p_{2,2} \ldots p_{2,N-1} \, 0]$, $\vec{p}_3^T \equiv [p_{3,2} \ldots p_{3,N-1} \, 0]$, $\vec{g}_{n,1}^T \equiv [g_{n,1}(1) \ldots g_{n,1}(N-1)]$, $\vec{g}_{n,2}^T \equiv [g_{n,2}(1) \ldots g_{n,2}(N-2) \, 0]$, $\vec{g}_{n,3}^T \equiv [g_{n,3}(1) \ldots g_{n,3}(N-2) \, 0]$, $g_{n,1}(j) \equiv X_{j,s_{n,j}}^2$ for $j \in [1, N-1]$, $g_{n,2}(j) \equiv (\vec{c}_j^T \vec{x}_{n,j} + \imath \, \vec{d}_j^T \vec{x}_{n,j})^2$ and $g_{n,3}(j) \equiv (\vec{c}_j^T \vec{x}_{n,j} + \imath \, \vec{d}_j^T \vec{x}_{n,j}) X_{j+1,s_{n,j+1}}$ for $j \in [1, N-2]$, and $g_{n,2}(N-1) \equiv g_{n,3}(N-1) = 0$. Then, by utilizing (A20), the following is obtained easily:

$$\chi_{T,N-1} = \chi_0 \prod_{j=1}^{N-1} \sqrt{\xi_j}$$
$$\times \exp\left\{ \vec{p}_1^T \left(\vec{x}_{n,N-1} \odot \vec{x}_{n,N-1} \right) \right\}$$
$$\times \exp\left\{ \vec{p}_2^T \left((\mathbf{G} \, \vec{x}_{n,N-1}) \odot (\mathbf{G} \, \vec{x}_{n,N-1}) \right) \right\} \tag{A24}$$
$$\times \exp\left\{ \vec{p}_3^T \left((\mathbf{G} \, \vec{x}_{n,N-1}) \odot (\mathbf{E}_1 \, \vec{x}_{n,N-1}) \right) \right\}$$

where $\odot$ denotes the point-wise product, and $\mathbf{G}$, $\mathbf{E_1}$, $\mathbf{E_2}$ and $\mathbf{V}_L$ are defined as follows:

$$\mathbf{V}_L \equiv \begin{bmatrix} \vec{v}_{0,1} & \mathbf{0_2} & \ldots & \mathbf{0_2} \\ \vec{v}_{0,2} & \vec{v}_{1,2} & \ldots & \mathbf{0_2} \\ \vdots & \vdots & \vdots & \vdots \\ \vec{v}_{0,N-2} & \vec{v}_{1,N-2} & \ldots & \vec{v}_{N-3,N-2} \end{bmatrix} \quad \text{(A25)}$$

$$\mathbf{E}_1 \equiv \begin{bmatrix} \mathbf{0_{N-2}} & \mathbf{I_{N-2}} \\ 0 & \mathbf{0_{N-2}^T} \end{bmatrix}; \quad \mathbf{G} \equiv \begin{bmatrix} \mathbf{E_2 V}_L & \mathbf{0_{N-2}} \\ \mathbf{0_{N-2}^T} & 0 \end{bmatrix} \quad \text{(A26)}$$

$$\mathbf{E}_2 \equiv \begin{bmatrix} 1 & \imath & 0 & 0 & \ldots & 0 & 0 \\ 0 & 0 & 1 & \imath & \ldots & 0 & 0 \\ \vdots & \vdots & \vdots & \vdots & \vdots & \vdots & \vdots \\ 0 & 0 & 0 & 0 & \ldots & 1 & \imath \end{bmatrix} \quad \text{(A27)}$$

while $\mathbf{0_k}$ is the column vector of zeros of length k, the sizes of $\mathbf{E}_2$ and $\mathbf{V}_L$ are $(N-2) \times (2N-4)$ and $(2N-4) \times (N-2)$, respectively, and $\mathbf{G}$ and $\mathbf{E}_1$ are $(N-1) \times (N-1)$.

Appendix B

The expression $\sum_{k=1}^3 \vec{p_k}^T \big((\mathbf{M}_{1,k}\, \vec{x}_n) \odot (\mathbf{M}_{2,k}\, \vec{x}_n) \big)$ equals to the following:

$$\overset{1}{=} \sum_{k=1}^3 \mathbf{Tr}\Big\{ \mathrm{diag}\{\vec{p_k}\}\, \mathbf{M}_{1,k}\, \vec{x}_n\, \vec{x}_n^T\, \mathbf{M}_{2,k}^T \Big\} \quad \text{(B1)}$$

$$\overset{2}{=} \sum_{k=1}^3 \mathbf{Tr}\Big\{ \mathbf{M}_{2,k}^T\, \mathrm{diag}\{\vec{p_k}\}\, \mathbf{M}_{1,k}\, \vec{x}_n\, \vec{x}_n^T \Big\} \quad \text{(B2)}$$

$$\overset{3}{=} \mathbf{Tr}\Big\{ \Big(\sum_{k=1}^3 \mathbf{M}_{2,k}^T\, \mathrm{diag}\{\vec{p_k}\}\, \mathbf{M}_{1,k} \Big) \vec{x}_n\, \vec{x}_n^T \Big\} \quad \text{(B3)}$$

$$\overset{4}{=} \mathbf{Tr}\Big\{ \vec{x}_n^T \Big(\sum_{k=1}^3 \mathbf{M}_{2,k}^T\, \mathrm{diag}\{\vec{p_k}\}\, \mathbf{M}_{1,k} \Big) \vec{x}_n \Big\} \quad \text{(B4)}$$

where $\mathbf{Tr}\{.\}$ is the trace operator. The equality $\overset{1}{=}$ is obtained by transforming the inner and point-wise product combination into a trace operation. $\overset{2}{=}$ and $\overset{3}{=}$ are due to the permutation and the addition properties of the trace operation, respectively, while $\overset{4}{=}$ is due to the permutation property. Then, the quadratic form results in (8).

Appendix C

The intensity at $\widetilde{k} - k$ for $k \in [1, \widetilde{k}]$ is as follows:

$$\widetilde{I}[\widetilde{k} - k] \overset{1}{=} \left| \sum_{n=0}^{N_p-1} g_3[n] e^{g_1[n]\,(\widetilde{k}-k)} e^{-\frac{\imath\, 2\,\pi\, \widetilde{G}_2[n]\, k}{\widetilde{k}}} \right|^2 \quad \text{(C1)}$$

$$\overset{2}{<} \left| \sum_{n=0}^{N_p-1} g_3[n] e^{g_1[n]\,(\widetilde{k}-k)} \right|^2 \quad \text{(C2)}$$

$$\overset{3}{<} \left| \sum_{n=0}^{N_p-1} g_3[n] e^{g_1[n]\,\widetilde{k}} \right|^2 = \widetilde{I}[\widetilde{k}] \quad \text{(C3)}$$

where $\overset{1}{=}$ is due to the definition in (11) and the first condition in Theorem 1, $\overset{2}{<}$ and $\overset{3}{<}$ are due to the second condition in Theorem 1.

Appendix D

The conditional probability for the sample at k_p is given by the following:

$$p(\widetilde{I}_n[k_p]|\widetilde{k}) = \frac{1}{\sqrt{2\,\pi\,\widetilde{\sigma}_p^2}} e^{-\frac{(\widetilde{I}_n[k_p] - \widetilde{I}[k_p])^2}{2\,\widetilde{\sigma}_p^2}} \quad \text{(D1)}$$

where $\widetilde{\sigma}_p \equiv \widetilde{\sigma}[k_p]$. Then, denoting $\vec{\widetilde{\boldsymbol{I}}}_n = [\widetilde{I}_n[k_0] \ldots \widetilde{I}_n[k_{M-1}]]^T$ and $\vec{\widetilde{\boldsymbol{I}}} = [\widetilde{I}[k_0] \ldots \widetilde{I}[k_{M-1}]]^T$, the log likelihood function is given as follows:

$$\log\big(p(\vec{\widetilde{\boldsymbol{I}}}_n|\widetilde{k})\big) = -\frac{M}{2}\log(2\,\pi) - \frac{1}{2}\sum_{p=0}^{M-1}\log(\widetilde{\sigma}_p^2)$$
$$- (\vec{\widetilde{\boldsymbol{I}}}_{n,\widetilde{\sigma}} - \vec{\widetilde{\boldsymbol{I}}}_{\widetilde{\sigma}})^T \cdot (\vec{\widetilde{\boldsymbol{I}}}_{n,\widetilde{\sigma}} - \vec{\widetilde{\boldsymbol{I}}}_{\widetilde{\sigma}}) \quad \text{(D2)}$$

where $\widetilde{I}_{n,\widetilde{\sigma}}[k_p] = \widetilde{I}_n[k_p] / (\widetilde{\sigma}_p\,\sqrt{2})$ and $\widetilde{I}_{\widetilde{\sigma}}[k_p] = \widetilde{I}[k_p] / (\widetilde{\sigma}_p\,\sqrt{2})$. Fisher information matrix denoted by $I_F[\widetilde{k}] \equiv E\big\{\big(\delta\log\big(p(\vec{\widetilde{\boldsymbol{I}}}_n|\widetilde{k})\big)/\delta\widetilde{k}\big)^2\big\} = -E\{\delta^2\log(p(\vec{\widetilde{\boldsymbol{I}}}_n|\widetilde{k}))/\delta\widetilde{k}^2\}$ for the zero mean random variable at each sample point is obtained after simple calculations as follows:

$$I_F[\widetilde{k}] = \sum_{p=0}^{M-1} \frac{1}{\widetilde{\sigma}_p^2} \left(\frac{\delta\widetilde{I}[k_p]}{\delta\,\widetilde{k}} \right)^2 \quad \text{(D3)}$$

which depends on the square of the derivative of the intensity on the period $\widetilde{k}$. Then, assuming an estimation method denoted by $\widehat{k}$ has a bias $b(\widehat{k}) \equiv E\{\widehat{k}\} - \widetilde{k}$, the Cramer-Rao Bound, i.e., $CR(\widetilde{k})$, for the variance of estimation is given by the following equality:

$$\mathrm{Var}(\widehat{k}) \geq CR(\widetilde{k}) = \frac{(1 + \delta b(\widehat{k})/\delta\widehat{k})^2}{I_F[\widetilde{k}]} \quad \text{(D4)}$$

$$= \frac{(1 + \delta b(\widehat{k})/\delta\widehat{k})^2}{\sum_{p=0}^{M-1} \frac{e^{4\,A_{N-1}\,(k_p\,T_s)^2}}{\sigma_p^2} \left(\frac{\delta\widetilde{I}[k_p]}{\delta\,\widetilde{k}} \right)^2} \quad \text{(D5)}$$

Furthermore, assuming $\sigma_p^2 \leq \sigma_{max}^2$, the maximum of the minimum variance bound is given by the following:

$$CR(\widetilde{k}) \leq \frac{\sigma_{max}^2\,(1 + \delta b(\widehat{k})/\delta\widehat{k})^2}{\sum_{p=0}^{M-1} e^{4\,A_{N-1}\,(k_p\,T_s)^2}\,(\delta\widetilde{I}[k_p]/\delta\,\widetilde{k})^2} \quad \text{(D6)}$$

while $\delta\widetilde{I}[k_p]/\delta\,\widetilde{k}$ is as follows:

$$\frac{\delta\widetilde{I}[k_p]}{\delta\,\widetilde{k}} = \sum_{n=0}^{N_p-1}\sum_{l=0}^{N_p-1} g_3[n]\,g_3^*[l]\,e^{(g_1[n] + g_1[l])k_p}$$
$$\times\,e^{-\Delta G_2[n,l]\frac{\imath\,2\,\pi\,k_p}{\widetilde{k}}} \left(\Delta G_2[n,l]\frac{\imath\,2\,\pi\,k_p}{\widetilde{k}^2} \right) \quad \text{(D7)}$$

Appendix E

The evolution of the wave function in nth path after the exotic travels of k slits as shown in Fig. 3 is as follows:

$$\Psi_{n,j,k}^E(x_{j,k}^E) = \int_{x_j} f_{n,k}^E(x_{j,k}^E, x_j)\, \Psi_{n,j,0}^E(x_{j,0}^E)\, \mathrm{d}x_j \quad \text{(E1)}$$

where $\Psi_{n,j,0}^E(x_{j,0}^E) \equiv G_{n,j}(x_j - X_{j,s_{n,j}})\, \Psi_{n,j}(x_j)$, $f_{n,1}^E(x_{j,1}^E, x_j) \equiv K(x_{j,1}^E, t_{j,1}^E; x_j, t_j)$ and $f_{n,k}^E(x_{j,k}^E, x_j)$ for $k \geq 2$ is defined as follows:

$$f_{n,k}^E(x_{j,k}^E, x_j) \equiv \int_{\vec{x}_{j;k}^E} \mathrm{d}\vec{x}_{j;k}^E\, K(x_{j,1}^E, t_{j,1}^E; x_j, t_j)$$

$$\times \prod_{p=2}^{k} K(x_{j,p}^E, t_{j,p}^E; x_{j,p-1}^E, t_{j,p-1}^E)\, G_{n,j}(x_{j,p-1}^E - X_{j,s_{n,j,p-1}})$$

$$\text{(E2)}$$

while $k \in [1, N_E]$, $k = 0$ case corresponds to the wave-function evolution without any exotic path, i.e., $\Psi_{n,j,0}^E(x_{j,0}^E)$, $t_{j,k}^E \equiv \sum_{p=1}^{k} t_{p-1,p}^E(j) + t_j$ is the time after visiting kth slit on jth plane, t_j corresponds to the time at the beginning of the exotic movements, $\vec{x}_{j;k}^E \equiv [x_{j,1}^E\ x_{j,2}^E\ \cdots\ x_{j,k-1}^E]$ and $x_{j,0}^E \equiv x_j$. Then, assuming that the nth path performs k consecutive visits to the slits on jth plane while the entrance slit is $X_{j,s_{n,j}}$ and the wave function at the position x_j is $\Psi_{n,j}(x_j)$, the wave function on the next plane, i.e., $\Psi_{n,j+1}(x_{j+1})$, becomes as follows:

$$\Psi_{n,j+1}(x_{j+1}) = \int K(x_{j+1}, t_{j,k}^E + t_{j,j+1}; x_{j,k}^E, t_{j,k}^E)$$

$$\times G_{n,j}(x_{j,k}^E - X_{j,s_{n,j,k}})\, \Psi_{n,j,k}^E(x_{j,k}^E)\, \mathrm{d}x_{j,k}^E$$

$$\text{(E3)}$$

REFERENCES

[1] R. P. Feynman, A. R. Hibbs, and D. F. Styer, *Quantum Mechanics and Path Integrals*, emended ed. (Dover Publications, Mineola, New York, USA, 2010).

[2] N. C. Jones, R. VanMeter, A. G. Fowler, P. L. McMahon, J. Kim, T. D. Ladd, and Y. Yamamoto, Phys. Rev. X **2**, 031007 (2012).

[3] R. D. Somma, D. Nagaj, and M. Kieferova, Phys. Rev. Lett. **109**, 050501 (2012).

[4] P. Bonderson, M. Freedman, and C. Nayak, Phys. Rev. Lett. **101**, 010501 (2008).

[5] A. Stern and N. H. Lindner, Science **339**, 1179 (2013).

[6] E. Gelenbe, The Computer Journal **55**, 848 (2012).

[7] I. G. daPaz, C. H. S. Vieira, R. Ducharme, L. A. Cabral, H. Alexander, and M. D. R. Sampaio, Phys. Rev. A **93**, 033621 (2016).

[8] R. Sawant, J. Samuel, A. Sinha, S. Sinha, and U. Sinha, Phys. Rev. Lett. **113**, 120406 (2014).

[9] A. Sinha, A. H. Vijay, and U. Sinha, Scientific Reports **5**, 1 (2015).

[10] J. Q. Quach, Phys. Rev. A **95**, 042129 (2017).

[11] D. Bigourd, B. Chatel, W. P. Schleich, and B. Girard, Phys. Rev. Lett. **100**, 030202 (2008).

[12] J. F. Clauser and J. P. Dowling, Phys. Rev. A **53**, 4587 (1996).

[13] J. Summhammer, Phys. Rev. A **56**, 4324 (1997).

[14] A. Rangelov, Journal of Physics B: Atomic, Molecular and Optical Physics **42**, 021002 (2009).

[15] V. Tamma, H. Zhang, X. He, A. Garuccio, W. P. Schleich, and Y. Shih, Phys. Rev. A **83**, 020304 (2011).

[16] M. A. Nielsen and I. L. Chuang, *Quantum Computation and Quantum Information* (Cambridge University Press, 2010).

[17] H. Ozaktas, Z. Zalevsky, and M. A. Kutay, *The Fractional Fourier Transform with Applications in Optics and Signal Processing* (John Wiley and Sons, Chichester, UK, 2001).

[18] J. C. Lagarias, in *IEEE 23rd Annual Symposium on Foundations of Computer Science* (1982) pp. 32–39.

[19] Y. Meyer, *Beyond Quasicrystals: Quasicrystals, Diophantine approximation and algebraic numbers* (Springer, 1995) pp. 3–16.

[20] T. Zielinski and K. Duda, Metrology and Measurement Systems **18**, 505 (2011).